MOLTEN DROP DEPOSITION AND SOLIDIFICATION ON AN INCLINED PLATE

by

Virginie L.C. Bouvier

B.S.M.E. Tufts University, 1998

Submitted to the Department of Mechanical Engineering
in Partial Fulfillment of the Requirements
for the Degree of

Master of Science
in Mechanical Engineering

at the

MASSACHUSETTS INSTITUTE OF TECHNOLOGY

June 2000

Signature of Author_____
Department of Mechanical Engineering
May 12, 2000

Certified by_____
Ain A. Sonin
Professor, Mechanical Engineering
Thesis Supervisor

Accepted by_____
Ain A. Sonin
Chairman, Departmental Committee on Graduate Studies
Department of Mechanical Engineering

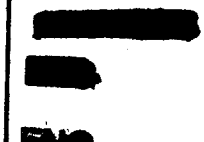

MOLTEN DROP DEPOSITION AND SOLIDIFICATION ON AN INCLINED PLATE

by

Virginie L.C. Bouvier

Submitted to the department of Mechanical Engineering on May 12, 2000 in partial fulfillment of the requirements for the Degree of Master of Science in Mechanical Engineering.

ABSTRACT

To develop new fabrication techniques by molten microdrop deposition processes requires an understanding of how the microdrops solidify upon deposition to form the building blocks. Previous theses in this laboratory have investigated the deposition and solidification of molten droplets on horizontal, cold solid surfaces (Gao, Ph.D., 1994; Schiaffino, Ph.D., 1996; Duthaler, Ph.D., 1999). The present thesis investigates the same problem with an emphasis on the deposition of molten drops on inclined surfaces.

Measurements of contact line position, contact angle, and contact angle velocity were obtained for approximately 300 depositions of molten octocosane droplets ($C_{28}H_{58}$) on glass microscope slides held at different temperatures. The apparent contact angle of the drop after it reaches arrest was studied as a function of the target temperature (expressed by the Stefan number, S) and the plate's angle of the inclination (denoted by γ). The results were roughly consistent with the previous studies (which were done with a microcrystalline wax) and were relatively weakly dependent on γ. The study of the dynamics of the drop's descent and its dependence on S and γ was complicated by the fact that there was a significant scatter of the data, that is, experiments with apparently the same initial conditions could give significantly different results for the drop's final length, velocity during descent, and apparent contact angle. Part of this problem may arise from the stick-slip behavior of an advancing contact line, first noted by Duthaler (Ph.D., 1999). The stick-slip behavior corresponds to momentary arrests of the contact line during its descent, followed by resumption of motion.

Thesis Supervisor: Professor Ain A. Sonin

Title: Professor of Mechanical Engineering

Acknowledgements

First, I would like to express my deepest gratitude to my advisor Professor Ain A Sonin. This work would not have been possible without his expert advice and patient guidance. It was a privilege for me to work with him.

I would also like to thank my friend and co-worker Pirouz Kavehpour and his wife Faranak Rahim for their help, kindness, and friendship.

I would also like to thank Claire Sasahara and Leslie Regan for their friendliness and essential administrative help.

All of my friends deserve my sincerest gratitude for everything they did during these past two years. I do not know where I would be without their help, their support, and their kindness. Violaine, Vanessa, Erik, Dave, Mohsen and Denise, Charles and Gaby, Hélène, Holly, Mark, Nikos, Olga, Victor, Barry, Hesham, Jessica, Emily and to all my friends and co-workers at Tufts and MIT, thanks to all of you.

I would also like to thank Professor F. Nelson and Professor V. Manno, for helping awaken my interest in engineering and for their support and guidance through the years.

Lastly, I can never thank enough my parents, Mr. and Mme. Pascal Bouvier, and my sisters, Adeline, Marine and Charlotte, for their unconditional love, support, and patience. I would like to dedicate this work to them, I would have never been able to do it without them. Thank you so very much. A very special place in my heart will always be for Mr. and Mme. Georges André and Mr. Olivier André. I miss you.

This research was supported by the National Science Foundation under grant CTS-9523764 ("Molten Microdrop Deposition on cold surfaces: Role of non-equilibrium contact angle"). NSF Program: Fluid, Particulate, and Hydraulic Systems Program.

Table of Contents

List of figures

1- Introduction/previous work:

The deposition and solidification of drop is the basis to many industrial applications. Drop can be use as building blocks in three-dimensional microfabrication or rapid prototyping, or they can be used, for example, in microelectronics device packaging, where small drops of solder are used to create electrical connections needed in microchips. For each of these applications, it is important to understand and be able to predict the shape of each drop after deposition and solidification, so that, in turn, one can predict the final product and its physical properties.

It is in this context, and with these applications in mind, that research was done in this laboratory by Gao (Ph.D., 1994), Schiaffino (Ph.D., 1996), Torresola (MS, 1998), and Duthaler (Ph.D., 1999) on molten drop deposition and solidification on horizontal, cold, solid surfaces. In this thesis we will try to extend their work to deposition and solidification on inclined, cold, solid surfaces.

Before the work of Gao (1994), most work on the moving of contact lines considered only isothermal conditions, where the liquid and solid are at the same constant temperature. A lot of work has been done under these conditions since numerous applications, such as coating or lubrication, implied a very good understanding as well as modeling of the situation; good reviews of this work are described by Dussan (1979), or Kistler (1993). Under isothermal conditions, the fluid advances over the surface until it reaches the equilibrium angle θ_e, which can be calculated from Young's equation, a horizontal force balance at the contact line,

$$\sigma \cos\theta_e = \sigma_{sg} - \sigma_{sl} \qquad (1)$$

where σ is the surface tension associated with the liquid/gas boundary, σ_{sg} is the surface tension associated with the solid/gas boundary, and σ_{sl} is the surface tension associated with the solid/liquid boundary. For an advancing isothermal contact line the apparent angle will be greater than θ_e, and in the receding case it will be less than θ_e. However, the modeling of the flow field using continuum theory yields a shear-stress singularity at the contact line. Theoreticians have typically avoided this problem by either using a cut-off of the continuum model at molecular scale (Voinov, 1978), or introducing a small

"slip length" over which velocity slip occurs (Hocking, 1992). The first of these techniques yields the well-known relationship called the Hoffman-Tanner-Voinov law,

$$Ca = \kappa_H (\theta_a^3 - \theta_m^3) \qquad (2)$$

where κ_H is a coefficient that is weakly dependent on the length scale and which has been found to fit experiments fairly well for a value of κ_H of $1.3*10^{-2}$ rad^{-3}, θ_m is the slope of the free surface at the contact line evaluated at the molecular scale and is usually assumed to be approximately equal to θ_e, and θ_a is the apparent contact angle. Ca, is the capillary number corresponding to the ratio of viscous force to capillarity ones,

$$Ca = \frac{\mu U}{\sigma} \qquad (3)$$

with μ the absolute viscosity, U the velocity of the contact line, and σ the surface tension. Due to the impossibility to get rid of the shear-stress singularity at the contact line in a way that would completely satisfy all theoreticians, this work on the advance of the contact line under isothermal condition continues (see for example Goodwin and Homsy, 1990, and Veretennikov, Indeikina and Chang, 1998).

Gao and Sonin (1994) described the possibilities of micro-fabrication using as building blocks droplets of molten material. They described the deposition on a flat plate and derived an expression for the apparent contact angle based on the volume of the molten material and the conservation of mass:

$$\frac{r_b}{a} = \left[\frac{4\sin^3\theta_a}{(1-\cos\theta_a)^2(2+\cos\theta_a)} \right]^{1/3} \qquad (4)$$

where r_b is half of the extent of the drop, a is the radius of the drop before impact and, θ_a is the apparent angle. They also derived expression describing the time scales of solidification and characterized columnar and sweep deposition for molten drop, and noted instabilities in high frequency bead deposition. The instabilities appeared to be related to Rayleigh's instabilities of cylindrical liquid shape.

It was not until the work done by Schiaffino and Sonin (1996) that an analysis of the molten contact line problem was done. The molten contact line is a very different problem from the isothermal one since non-equilibrium processes control it. It is the solidification process that determines the dynamic of the contact angle as well as the

conditions for the contact line arrest. Schiaffino and Sonin (1997) developed scaling laws that described the solidification processes and they showed that the apparent contact angle is primarily dependent on the difference between the fusion temperature and the target temperature, through the Stefan number, defined as,

$$S = \frac{c_p (T_f - T_t)}{h_{fg}} \qquad (5)$$

where c_p is the specific heat of the molten material, T_f is the fusion temperature, T_t is the target temperature, and h_{fg} is the latent heat of fusion of the molten material. When Schiaffino and Sonin (1997) tried to solve for the conventional formulation of the heat transfer equations that describes this problem, they were faced with a heat flux singularity at the contact line. They were able to solve, however, for the cut-off length, defined as the length near the contact line within which the conventional model shows inconsistencies between the calculations and the experiments. They also showed that under certain circumstances the contact line motion during the spreading of the melt agreed with a particular form of the Hoffman-Tanner-Voinov law, equation 2.

Duthaler (1999) followed up on this work. He obtained data describing the arrest conditions for different materials than the one studied by Gao (1994) or Schiaffino (1996), and developed a theoretical model of the molten contact line advance on a cold flat surface that enables prediction of the velocity-angle relationship. Though he was not able to resolve the contact line heat flux singularity, and approximated the solidification front as a "wedge-step", his theory seemed to be in good agreement with much of the experimental data he obtained. Duthaler also started looking at the inclined plate problem and noticed variations in the velocity of the molten contact line going down the inclined plate that seem to point toward the possible existence of a "stick-slip" behavior of the drop's advancing contact line.

The work we present here is a continuation of Duthaler's work on inclined plates. We measured the contact line position, contact angle, and contact angle velocity as a function of time on inclined, cold, solid surfaces. Specifically, we looked at the deposition of molten octocosane drops ($C_{28}H_{58}$) on a microscope glass surface. We did a total of 373 depositions and tried to make general statistical observations that would allow us to predict, based on specific parameters, the shape of the drop. We were faced

with the problem of the non-repeatability of the data, which was first mention for octocosane deposition by Torresola (1998), and tried to understand the origin of the variations noticed. For two apparently completely similar depositions, we obtained variations in final length, in arrest contact angles, and in general shape. As mentioned by Duthaler (1999), the possibility of a "stick-slip" behavior of the drop was also noticed in our experiments and the possibility that it could be linked to the problem of repeatability was raised. Based on the numerous experimental data obtained, we also attempted to correlate empirically the arrest contact angle measurements with the Stefan number, and the dynamic contact angles with the velocity measurements.

2- Material and method:

To investigate the deposition of drops on an inclined plate, we measured the angle that the contact line of a drop of molten material forms with the target surface as it goes down an inclined plate held below that material's freezing point. We restricted our interest to octocosane because unlike microcrystalline wax (e.g. Reed 6882 used by Gao (1994), and Schiaffino (1996)), octocosane has well-defined properties, and a distinct freezing point where the change of phase from solid to liquid happens abruptly. These conclusions were drown by Torresola (1998) as he identified the properties of Reed 6882 wax used in the model designed by Schiaffino and Sonin (1997) and compared it to octocosane. Octocosane is a long-chain paraffin: its chemical composition is $C_{28}H_{58}$. It has a fairly low fusion temperature of 61.4°C, which allows an easy experimental set-up.

2.1 – Material:

The depositions were done here on glass microscope slides. This influenced the results, and should be kept in mind in our comparison with previous work in which depositions were done on target of the same material as the melt. Table 1 represents the properties of glass and octocosane (Torresola (1998)) that were used in our analysis:

Properties of glass:		
Fusion temperature T (°C),	T_f	1500
Solid density (kg/m^3),	ρ_s	2500
Thermal conductivity (W/m K),	k	1.4
Specific heat (J/kg K),	c_p	750
Thermal diffusivity (m^2/s),	$\alpha = k/(\rho c_p)$	$7.5*10^{-7}$
Properties of octocosane (Javier Torresola 02/05/98 MS-ME-MIT):		
Fusion temperature T (°C),	T_f	61.4
Solid density (kg/m^3),	ρ_s	804
Liquid density (kg/m^3),	ρ_l	774
Viscosity (mPa s),	μ	4.9
Kinematic viscosity (m^2/s)	$\nu=\mu/\rho$	$6.3*10^{-6}$
Surface tension (N/m),	σ	0.026
Thermal conductivity (W/m K),	k	0.15
Specific heat (J/kg K),	c_p	2378
Latent heat (kJ/kg),	h_{fg}	163.6 (at 61.4°C)
Thermal Diffusivity (m^2/s),	$\alpha=k/(\rho c_p)$	$7.9*10^{-8}$

Table 2.1.1 – Properties of glass and octocosane.

It should be noted that the thermal conductivity and diffusivity of glass are both about an order of magnitude larger for glass than for octocosane, which will affect the analysis of the molten contact line, and the contact line arrest.

2.2 – Method:

The experimental method has three main components. The first consist of depositing the drops of octocosane in a repeatable fashion and recording both the temperature of the molten material right before impact and the target temperature. The second consists of recording the shape of the sessile drop as it flows down the inclined plate using a camera. The third consists of analyzing the resulting film, frame by frame, and tracking the apparent angles of the drop, its size, and the advance of the contact line from one frame to the next so that the velocity and displacement can be calculated.

2.2.1 - Deposition of the drops:

To create the drop we use a conical aluminum crucible that is held at a fixed temperature above the melting point of the drop material (see Figure 2.2.1.1). A certain amount of small grains of solid octocosane is deposited into the crucible. This material will melt, flow down, and accumulate at the tip of the crucible's cone, forming the drop. When the weight of the drop becomes large enough, the drop detaches itself from the tip of the cone and falls on the solid inclined, cold glass surface below it. Due to the blur in the pictures, only an approximate value of the radius of the drop can be given, we found that the radius a of the drop before impact is 1.7 ± 0.2 mm, which yields a volume between 14 and 29 mm^3. An automated temperature controller (Omega CN76000 1/16 DIN Auto-Tune), a 100 W cartridge heater, and a type T thermocouple attached to the surface of the aluminum cone, control the crucible's temperature. The thermocouple gives a continuous reading of the temperature at the tip of the cone where the drop forms. This temperature is a good approximation of the temperature of the liquid drop as it detaches itself from the cone. Duthaler (1999) used the same apparatus to create the drops of octocosane he studied for both horizontal and inclined depositions.

The drop then falls from a height of approximately 10 millimeters onto a glass microscope slide, which is 1 millimeter thick. The glass is mounted on an aluminum plate and the contact between the glass and the aluminum plate is improved by the use of a thermally conductive paste. A temperature controller, a type T thermocouple, and flexible cartridge heaters control the temperature of the aluminum plate. The

thermocouple is placed at the upper surface of the aluminum plate and allows a continuous reading of surface temperature. Since glass is a good conductor and since we use a thermally conductive paste, we were able to use the temperature read by the thermocouple as an acceptable approximation of the target temperature. Several measurements of the temperature of the glass plate were compared to readings done of the aluminum plate temperature, and the difference was found to be ±0.5°C.

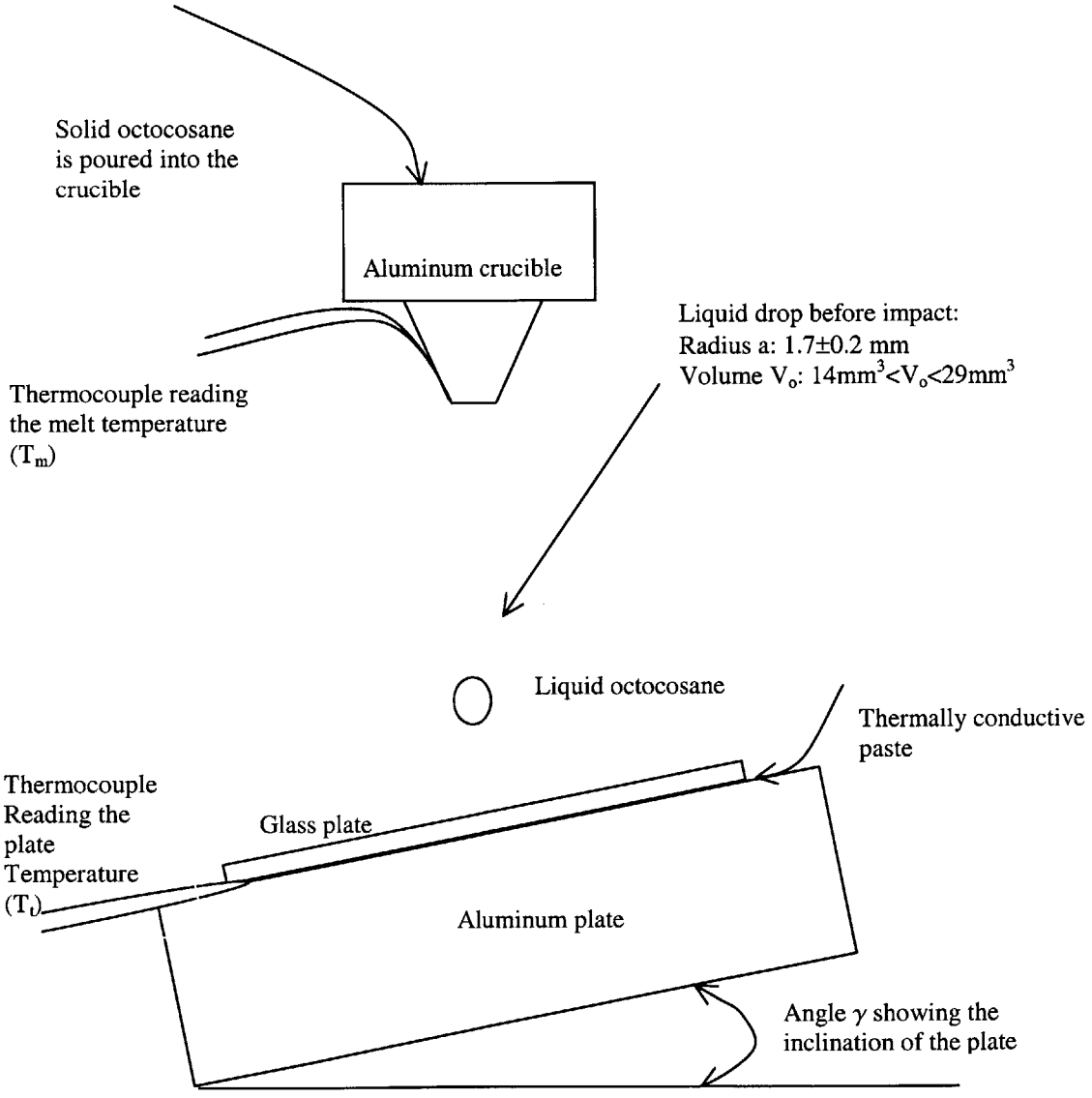

Figure 2.2.1.1 Schematic representation of the apparatus used

2.2.2 - Recording of the spreading of the drop:

During its descent we filmed the drop from the side. Depending on the experiment, one of two cameras was used: a CCD camera that allows recording at 30 frames per second, or a High Speed Camera (HSC). The HSC is a Kodak Ektapro EM Processor, Model 1012. Its recording rate ranges from 50 to 1,000 full frames per second. We used speeds of 500 and 1,000 frames per seconds, which yields an exposure time of 1/500 and 1/1,000 of a second respectively. The CCD camera was used first, to get a general idea of what is happening and of the maximum spreading of the drop, for each angle γ of the plate, and each Stefan number. The CCD camera was used mainly for precise very slowly evolving processes, because differentiating the frames cannot be done as accurately as with the HSC. The HSC, on the other hand, is more difficult to use because it requires very good lighting of the drop and because it can record no more than 2 seconds of the spreading process at 500 frames and 1.2 seconds at 1,000 frames per second. It would be possible, in principle, to increase the precision of the picture taken with the HSC by using a synchronized flash light, but that reduces the exposure time of each picture significantly. We were unable to use such a technique because the HSC needs very good lighting and we were not able to obtain suitable flash lights.

2.2.3 - Analysis of the films:

When using the HSC, each frame of the film is separated and sent to a computer where an image processor allows the user to magnify the picture and measure angles and distances. This technique has limitations. A picture is composed of pixels, the size of which is a measure of the minimum readable distance. Using the image processor, we measured the length of one pixel to be from 28 to 48 μm with the HSC (adjustable lens), and 7.2 μm with the CCD. When reading the total length of the spreading drop, we can not magnify the picture as much as we do when reading an angle because the totality of the drop needs to be seen at once on the screen. This limits the accuracy of the readings to about ± 200 μm for the HSC measurements.

The inaccuracy of the distance readings leads to similar limitations in the determination of the velocity of the molten contact line as it moves down the plate. Two different techniques are used. The first one consists of measuring for each frame the

length of the drop and comparing it to the length measured in the previous frame; however, the reading of the distance is then only accurate to ± 200 μm, which yields a maximum accuracy for the speed of ± 0.2 m/s. Since the average speed of the contact line will vary from 0.05 m/s to approximately 1 m/s, this technique is therefore not accurate enough for our purpose. The other technique uses the subtraction of two pictures. Prior to the subtraction we marked the contact line position of the drop on each frame with a point. The picture that results from the subtraction of two frames will show the two points (one in white, the other in black). It is then possible to measure the distance between these two points with the maximum magnification and therefore an accuracy of 48 μm with the HSC, which yields an accuracy of ± 0.048 m/s for the speed. It is also possible to look at a picture every 5 or 10 frames and get a correspondingly better accuracy in the velocity readings (e.g. an accuracy of ± 0.0096 m/s, for 5 frames, and of ± 0.0048 m/s, for 10 frames, at a frame rate of 1,000 frames a second).

Another problem encountered with the analysis of the picture is reading the angles. To read the angles one relies on the change of darkness of the pixels. Even at a frame rate of 1,000 per second (with the HSC), the drop motion between frames is not negligible and the boundaries are somewhat blurry. The precision of determining the angles is about ± 3° on average, and depends on the lighting conditions and the drop's average descent speed, which can vary from about 1 m/s to 0.05 m/s.

3- General observations:

This section shows a few examples of the deposition on surfaces inclined at different angles γ and at different plate temperatures (different S).

Figure 3.1 represents two drops deposited on a horizontal plate at different temperature. Based on the previous work on the deposition of molten drops (Gao and Sonin (1994)), we know that, the drop's shape depends primarily on the parameter S. For S=0.31 (left picture) the temperature of the plate is approximately 40°C and the drop takes approximately the shape of a spherical cap. For S=0.08 (right picture) the temperature of the plate is approximately 56°C, approaching the fusion temperature of the melt (T_f = 61.4°C), and the drop spreads to a smaller final contact angle and a greater drop diameter.

Figure 3.2 and 3.3 show the general shape with different inclination γ of the plate, in Figure 3.2 the plate is inclined at 15° and Figure 3.3 at 25 °. The two pictures were taken after final arrest was reached while bulk solidification was happening, which allows us to be sure that the angle that the contact line forms with the target will not change, and therefore that we are measuring $(\theta_a)_\infty$. We note that the profile is elongated in the direction of the descent. Upon impact with the plate the drop tends to wet the surface under the influence of capillarity forces and flows down the slope under the influence of gravity. The back, or tail, of the drop reaches arrest quickly, since the back contact line tries to recede, and is thereafter pinned to the surface. Then the drop stretches along the plate as the leading edge (or head) moves forward down the incline. Depending on several factors, the drop takes one of the final shapes shown in Figure 3.4. To reach the final shape on the right (b), the drop passes through the stage presented on the left (a). The top views are sketches of what is observes after solidification; the one represented in Figure 3.4 b shows changes of width which were observe primarily for deposition at high S.

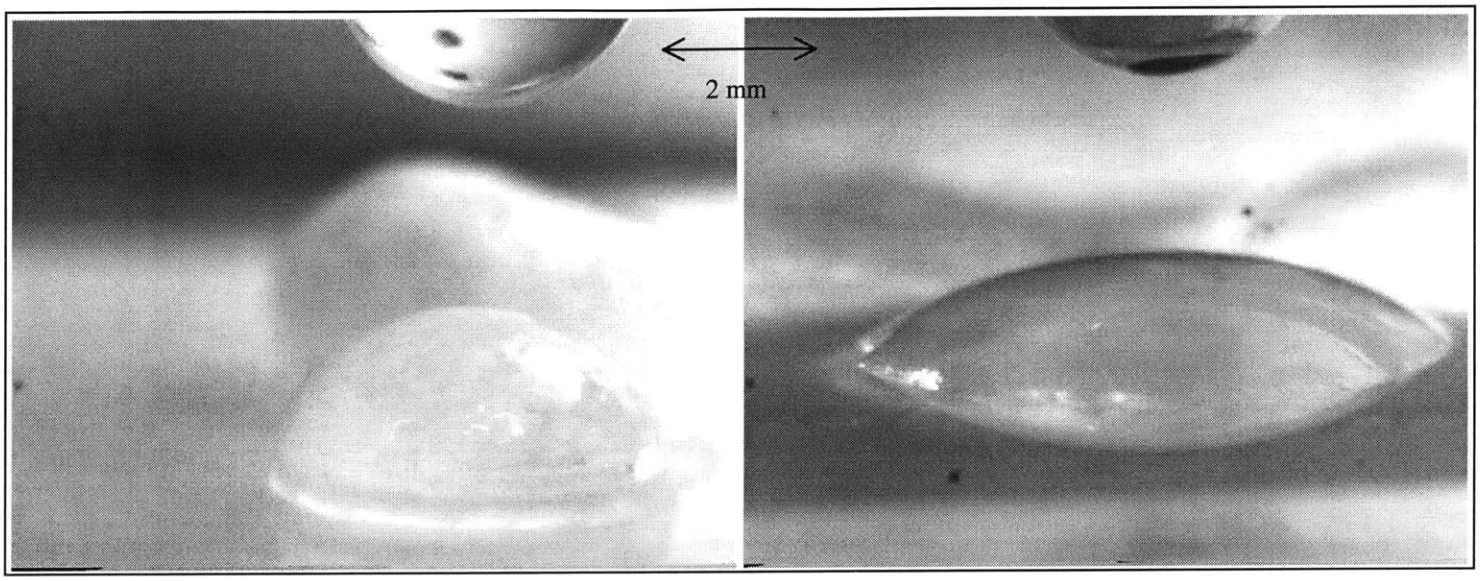

Figure 3.1 - Deposition on a horizontal plate
a) Left: CCD S=0.31, γ=0 (Run 179) after bulk solidification
b) Right: CCD S=0.08, γ=0 (run 266) after complete arrest, but before completion of bulk solidification
Note: -Picture a) has a higher S and therefore a larger arrest contact angle than picture b).

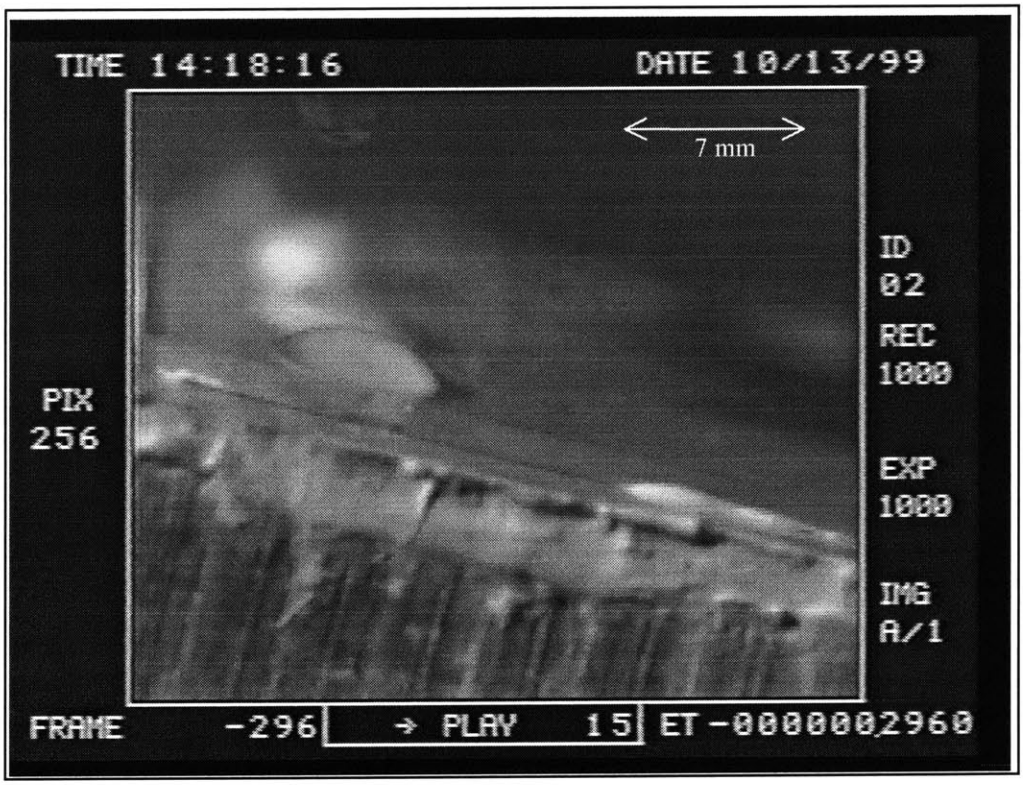

Figure 3.2 - Deposition on a plate inclined at 15°
HSC S=0.19, γ=15 (Run 367) after complete arrest, but before completion of bulk solidification

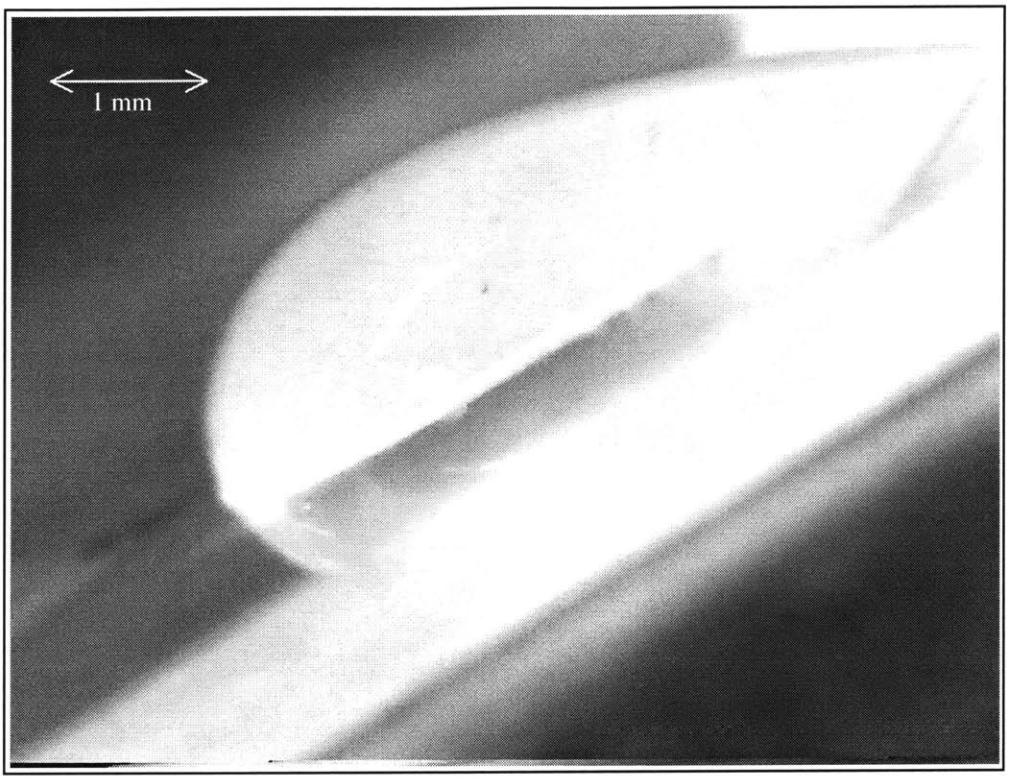

Figure 3.3 - Deposition on a plate inclined at 25°
CCD S=0.38, γ=25 (Run 97) after complete arrest, but before completion of bulk solidification
Note: the plate is inclined, the drop takes a tear like shape.

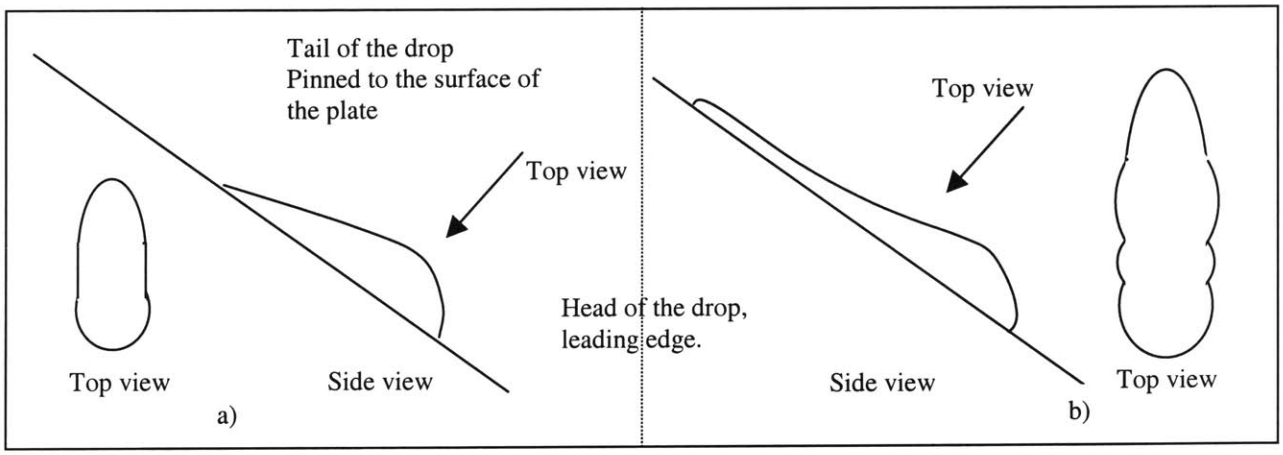

Figure 3.4 Schematic of the general shapes a drop.
Note: - to reach the shape in b), the drop will go through the stage presented in a).
- The top view in b) shows changes in width that can be observed on some solidified cases; due possibly to partial arrest of the drop or jumps in velocity.

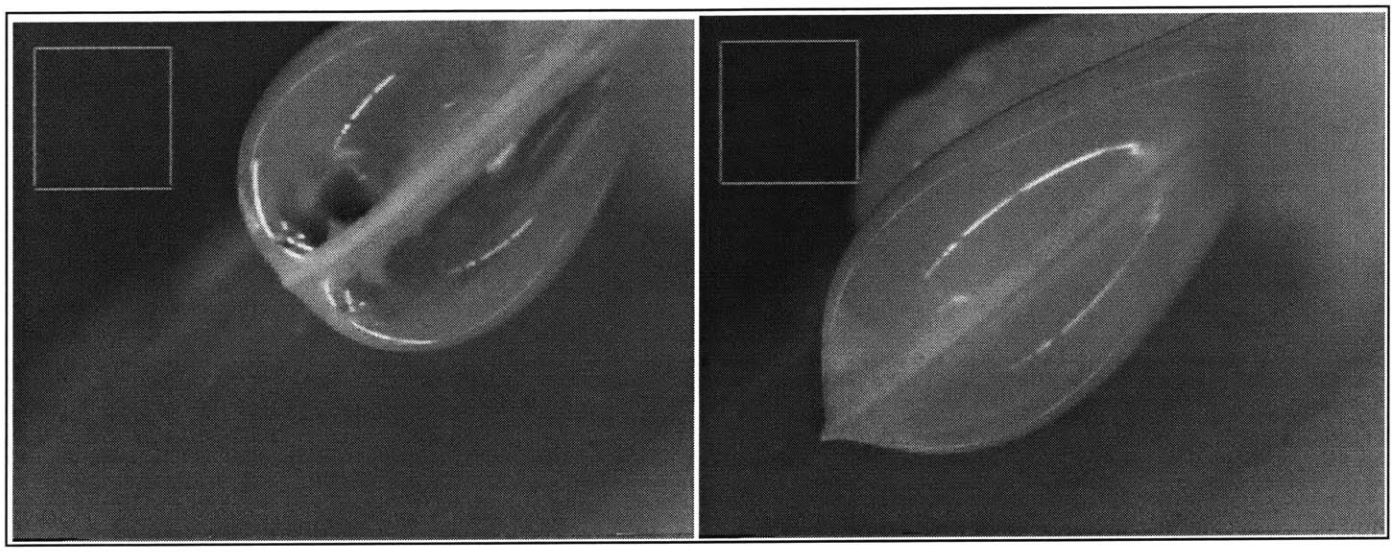

Figure 3.5 - Deposition on a plate inclined at 45°
a) Left: CCD S=0.31, γ=45 (Run 196) after complete arrest, but before completion of bulk solidification
b) Right: CCD S=0.31, γ=45 (Run 197) after complete arrest, but before completion of bulk solidification
Note: - the squares in both pictures have sides of approximately 1 mm.
-though the two depositions were done under similar conditions the arrest contact angles are very different.

Figure 3.6 - Deposition on a plate inclined at 45°
a) Left: HSC S=0.43, γ=45 (Run 317) after complete arrest, but before completion of bulk solidification
b) Right: HSC S=0.43, γ=45 (Run 321) after complete arrest, but before completion of bulk solidification
Note: - thought the two depositions were done under similar conditions the general shapes are very different.

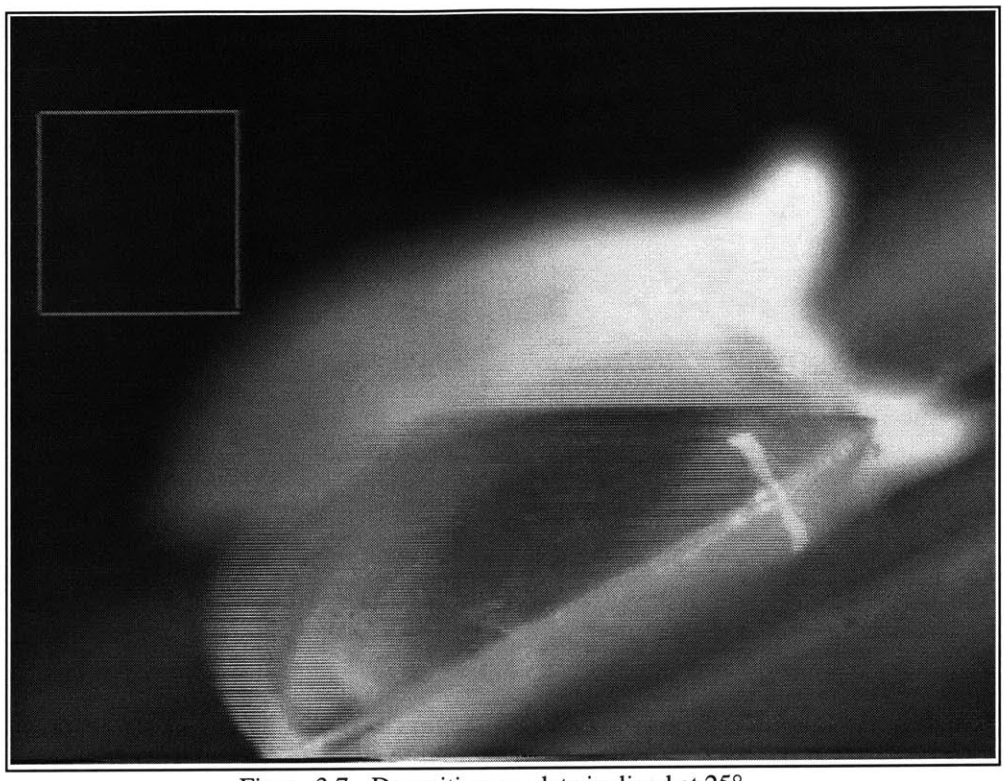

Figure 3.7 - Deposition on plate inclined at 25°
CCD S=0.52 γ=25 (Run 37) after reaching its final length but as it is still oscillating to reach its final angle
Note: the square in the picture has sides of approximately 1 mm
the oscillation of the drop as it settled down to a final shape

Figure 3.8 - Solidified drop plate inclined at 25°
CCD S=0.53 γ=25 (Run 29) after bulk solidification
The square in the picture has sides of approximately 1 mm.
Note: - during the solidification octocosane shrinks down and a dimple on the top of the solidified drops forms.

Based on the observations done for deposition on a horizontal plate, we expected that for a drop of given diameter, a (or volume, V_o), the drop's shape (Figure 3.6) and the contact angle (Figure 3.5) should be determined by the inclined angle (γ) and the sub-cooling temperature of the target (through the Stefan number, S). However, the inertia of the drop going down the incline and gravity forces and the solidification process and other factors such as the drop's post-impact oscillation at its natural frequency, also influence the final shape. This can be seen in Figure 3.5 which shows two drops deposited under apparently the same conditions (same angle of the plate γ, same S). The final shapes are however different, with a much smaller final contact angle for picture (b). Similarly, Figure 3.6 shows two drops deposited under the same conditions, but the one in Figure 3.6 (a) reached arrest earlier (in time and space) and takes a shape similar to the one represented in Figure 3.4 (a), while the one on the right (Figure 3.6 (b)) stretches along the plate and reaches a shape similar to the one represented in Figure 3.4 (b).

Figure 3.7 shows the oscillations that the drop experiences during the descent. These oscillations are particularly important once the drop has reached its final length and is settling into its final shape. All pictures taken with the CCD camera before an equilibrium position is reached will resemble Figure 3.7, i.e. the oscillations and advance of the contact line make the picture blurry, and therefore a precise length or angle will be very inaccurate. This is why a HSC was used for the entire dynamic analysis presented here.

Figure 3.8 shows a drop after completion of the solidification process. Note the small dimple on the top of the drop, which is a characteristic of materials like octocosane that shrink during solidification

4- Experimental results:

4.1 - Comparison between two runs/the problem of repeatability:

The first thing that appears from our data, for deposition and spreading of a molten octocosane drop on an incline glass plate, is the scatter, or lack of reproducibility.

From previous work done by Duthaler (1999) using the same apparatus (crucible, target, temperature controllers), it was concluded that the deposition itself, the creation of the drop from the melting of solid octocosane in the crucible, is a repeatable phenomenon, and that the volume of octocosane deposited each time by the crucible is also fairly repeatable ($14<V_o<29$ mm^3). Such a conclusion was reached by measuring the satellite drop that are created each time and which bounces off of the main drop. They were found to have a similar size each time. However that may be, the results we obtained experimentally did not seem as repeatable as we would have expected them to be, or as deposition on horizontal plates are. When depositing drops under the exact same conditions (target temperature, melt temperature, ambient temperature (S and β), angle of the incline plate (γ), and even same microscope glass slide) the results could sometimes show very little repeatability.

Figure 4.1.1 shows the extent of the drop (L) as a function of time for two runs at apparently identical initial conditions: $\gamma = 45°$, S=0.43, β=0.94. Time zero was adjusted so as to bring both data sets into coincidence during the early part of the spreading.

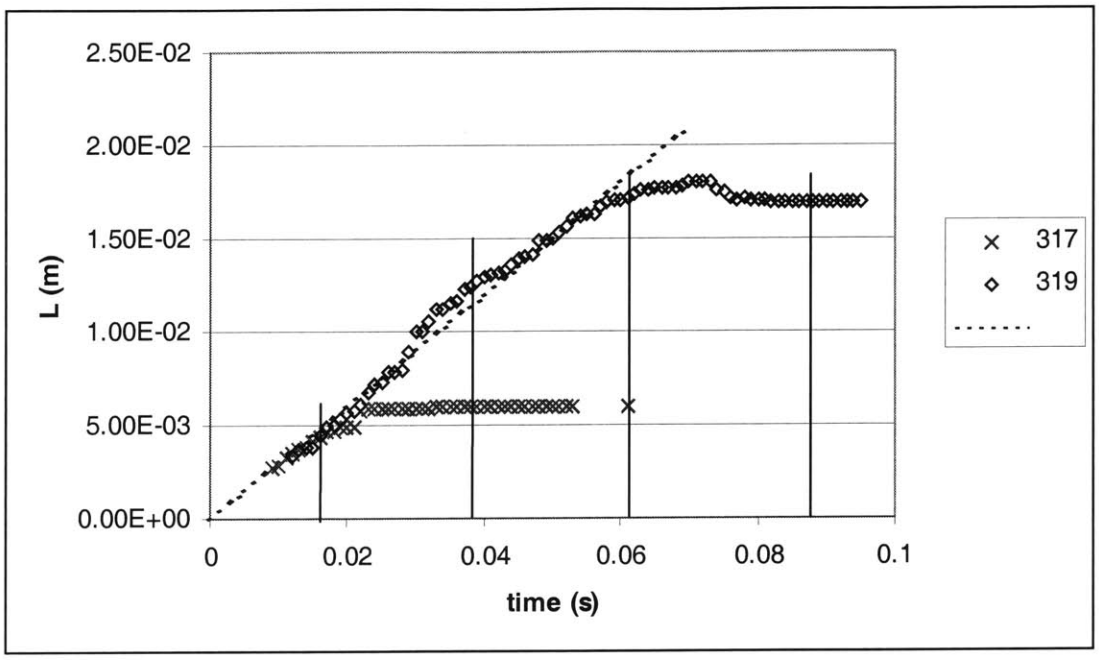

Figure 4.1.1 - Length of the drop, L (m) as a function of time (s), for two different depositions. (run 317 and 319). both executed with: γ=45°, S=0.43
The vertical lines represents the time of the different pictures presented in Figure 4.1.2 (a) and (b).

We note that the leading edge of the molten octocosane has two different stages of advance: a rapid advance at approximately constant speed, followed by a deceleration and arrest. Gravitational, capillarity, inertia, and viscous forces will control the rapid advance, while we believe that the deceleration and arrest is controlled by the melt freezing in the near contact line region. Although the two depositions were run under apparently similar conditions, they differ significantly in that run 317 arrests much sooner than run 319. This results in a significant difference in final length, the final length of run 319 being more than twice the one of run 317 (Figure 4.1.1 and the top view pictures presented in Figure 4.1.2 (a) and (b)).

Figure 4.1.2 (a) run 319. Picture of the drop's spreading.

t = 0.016s $t/\tau = 1.04$

t = 0.039s $t/\tau = 2.53$

t = 0.062s $t/\tau = 4.02$

t = 0.09s $t/\tau = 5.83$

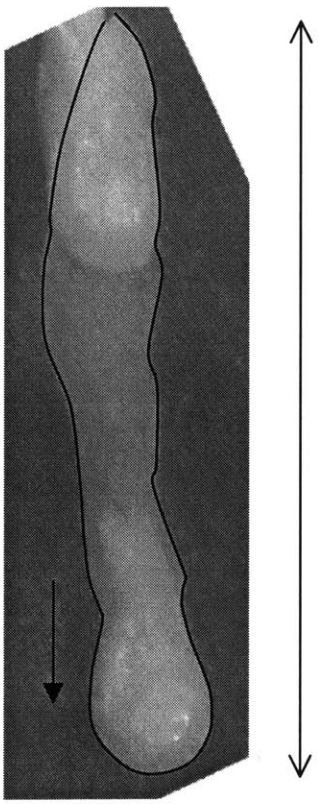

17 mm
L/a = 8.5

TOP VIEW - Picture from the top taken after complete solidification of the drop.
Note that the picture are taken from above and that in this case the drop solidify with a bulk angle greater than $\pi/2$ making it impossible to see the leading contact line.

Figure 4.1.2 (b) run 317. Picture of the drop's spreading.

t = 0.016s $t/\tau = 1.04$

t = 0.039s $t/\tau = 2.53$

t = 0.061s $t/\tau = 3.95$

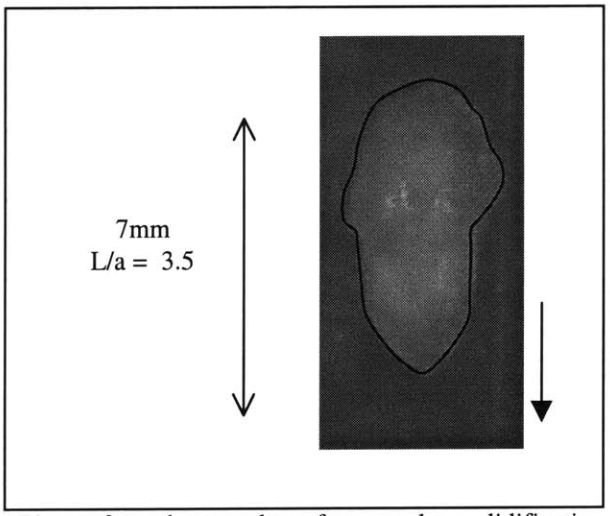

TOP VIEW - Picture from the top taken after complete solidification of the drop.
Note that in this case the bulk angle is less than $\pi/2$, therefore allowing us to see the leading edge of the drop.

A comparison between Figures 4.1.2 (a) and (b) shows several differences and similarities. Tough the three first pictures in (a) and (b) were taken at approximately the same times (time zero was obtained by matching the two profiles in Figure 4.1.1), we note that only the first frame (t=0.016s) have approximately similar general shapes. The third frame differs because, while run 317 has reached arrest, run 319 is still moving, approaching its deceleration zone (Figure 4.1.1, third vertical line). The second pictures look somewhat similar, but also have some differences. Both drops appear to have two parts: the bulk of the fluid that is pulling the drop downward, and a tail. In run 319, the tail is longer than the bulk of the fluid (or head of the drop), which takes a balloon shape and is separated from the tail. In run 317 there is no distinct head and tail, just an elongated drop with a tear like shape. From Figure 4.1.5 and 4.1.6, we note that the average velocity is actually larger for drop 319 (0.3 m/s versus 0.23 m/s), which would be the cause for the length difference between the two drops at t=0.039s (second pictures in Figure 4.1.2 (a) and (b)). From a comparison between the third and fourth pictures of run 319, we see that the head of the drop seems to be pulling forward in the third picture while it seems at rest in the fourth. In the third picture the bulk of the liquid forms an angle greater than $\pi/2$ with the target surface, while in the fourth picture it is closer to $\pi/2$ (Figure 4.1.5 (a)). In the picture taken from above of the solidified drop we note that because this angle is greater than $\pi/2$ in run 319, we do not see the leading edge and the solidified contact line as we do in run 317.

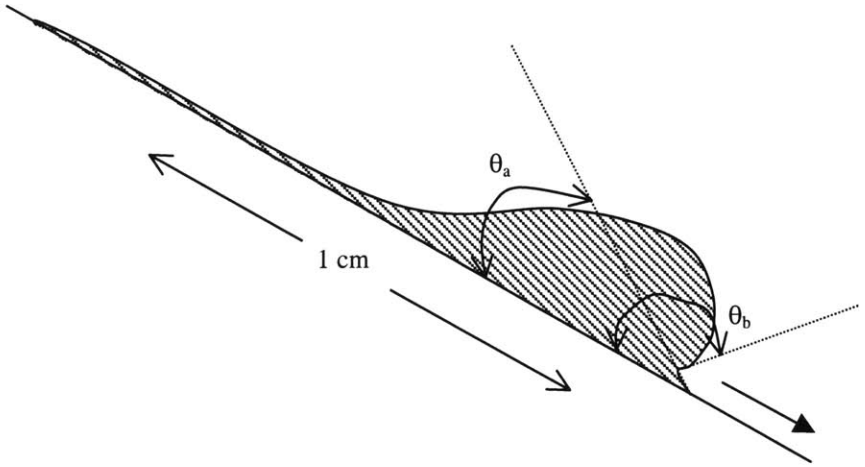

Figure 4.1.3 Representation of the drop's two angles θ_a and θ_b.

During its descent along the cold solid glass surface, the drop takes a general shape that sometimes shows two apparent contact angles, as shown in Figure 4.1.3. We denote by θ_b the bulk liquid contact angle and by θ_a the apparent contact angle. Where θ_a is the angle measured at a much smaller scale (approximately 100 μm) then θ_b, therefore a greater magnification is needed to be able to measure it properly, as shown in Figure 4.1.3 and 4.1.4. θ_b is more representative of the general shape of the drop while θ_a represents the advance (change of velocity) of the drop and would be more closely linked to the solidification angle especially in the near-arrest stages of the drop (Duthaler, 1999). Our understanding of the phenomenon that takes place here is that, as the drop goes down the incline plate, it also slowly solidifies. The solidification layer starts from the glass surface and thickens as time goes by. Due to the heat flux singularity that the conventional analysis of the heat transfer yields in this case, we do not know exactly the shape of the solidification layer. We expect it, however, to take a wedge-like shape at the contact line, to have an angle θ_s, and for the molten contact line to have a larger apparent angle (Schiaffino and Sonin, 1997, and Duthaler, 1999).

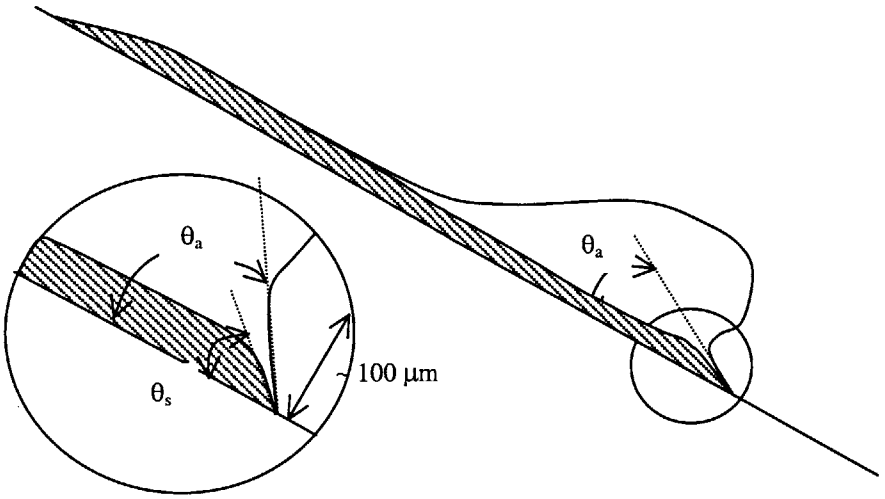

Figure 4.1.4 Representation of the drop's estimated solidification layer, θ_s.

θ_s however, is unknown and we expect it to be at a scale of order 10^{-1} μm for small S (Schiaffino and Sonin, 1997). Both θ_a and θ_b are important if one is to understand what is going on during the advance and solidification of the drop; they seem to be linked, and sometimes coincide perfectly. They also should be related to θ_s, and in that regard could give us information on the solidification profile that seems to control much of the dynamics and arrest of the drop.

Figure 4.1.5 shows the data obtained for run 319. This Figure shows the two angles versus time; the link between them is apparent in this case, for the two angles reunite (at time t = 0.083s) as the drop settles into a final shape (when the oscillation starts to damp out) but separate again after approximately 0.01s. We note that during the drop's advance and during most of the oscillations that occurs after reaching a final length, the difference between the two angles is approximately constant at 80°.

During the advance of the drop we can calculate an average velocity of the molten contact line based on the change of extent of the drop as a function of time,

$$\frac{\Delta L}{\Delta t} \cong \frac{dL}{dt} \equiv v \qquad (6)$$

In the case of run 317 (Figure 4.1.5 (b)) the average velocity is approximately 0.3m/s. From Figure 4.1.5 (b) we note that the change of length of the drop in time shows oscillations and even possible partial arrest at time at time t = 0.026s and 0.05s.

Figure 4.1.6 shows similar data for run 317. The difference between the two angles during the drop's advance is also approximately constant at 80° (Figure 4.6 (a)) but starts to decrease once the drop has reached its final extent (see Figure 4.1.6 (b) and Figure 4.1.1), which is at the same time as the oscillation starts to damp out and the drop is reaching an equilibrium position. At time t = 0.042s the difference disappears entirely in contrast to Figure 4.1.5. The angles do not separate again, and solidify at a common value.

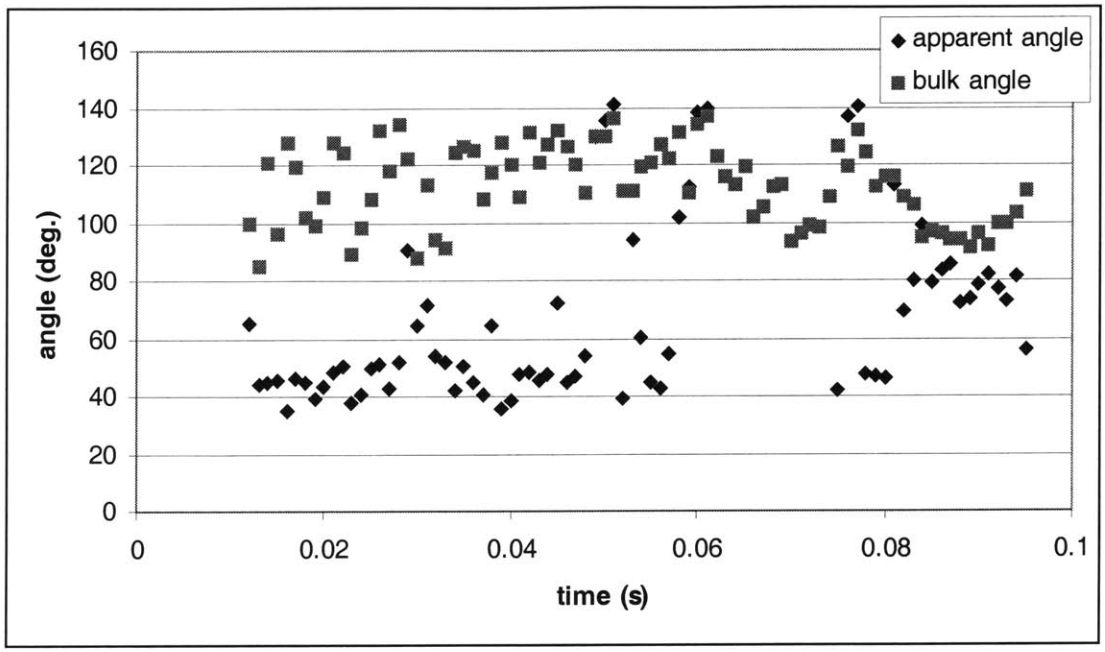

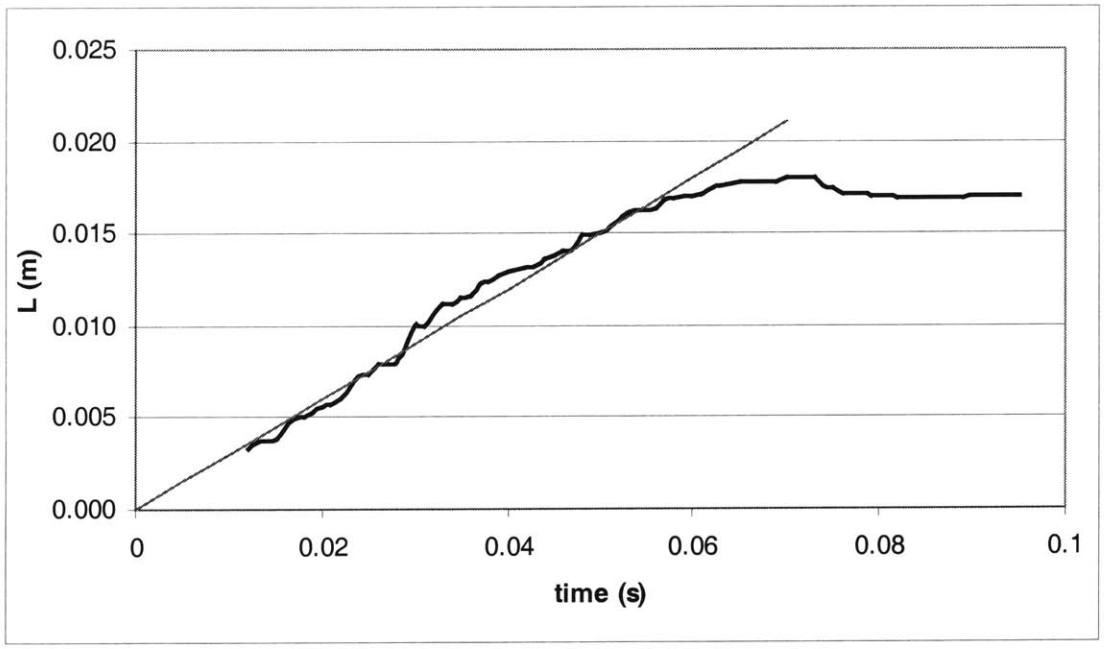

Figure 4.1.5 Drop deposited on an inclined plate ($\gamma = 45°$)
(Run 319 - S=0.43 – Also see Figure 4 .1.2 (a)).
(a) Top: Angle (deg.) versus time (s)
(b) Bottom: Length of the drop L (m) versus time (s)

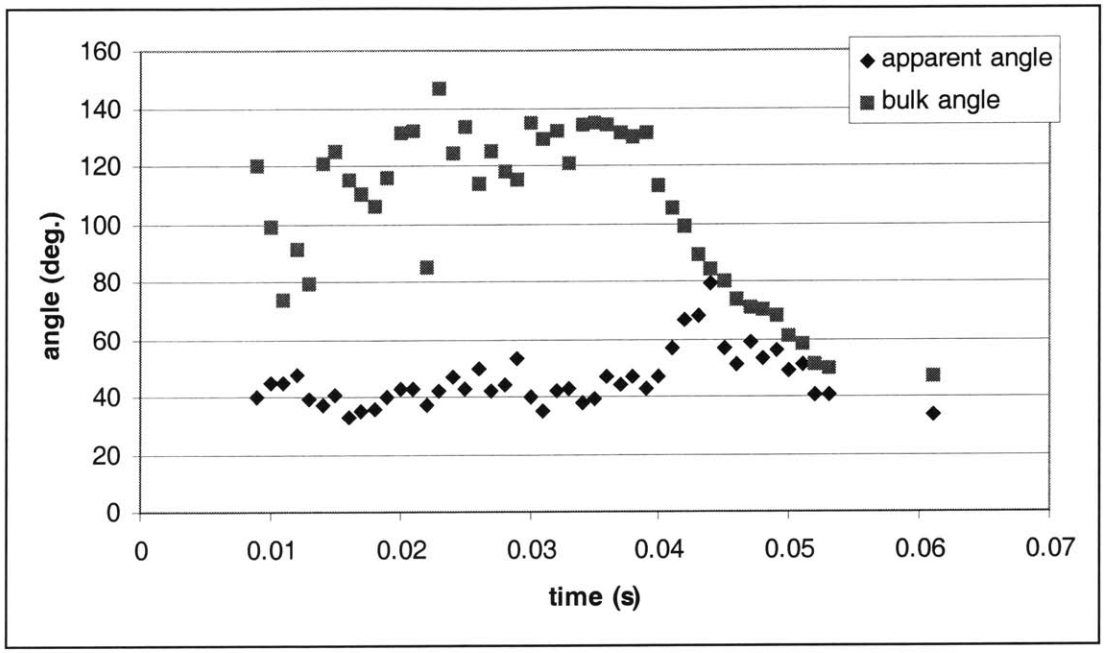

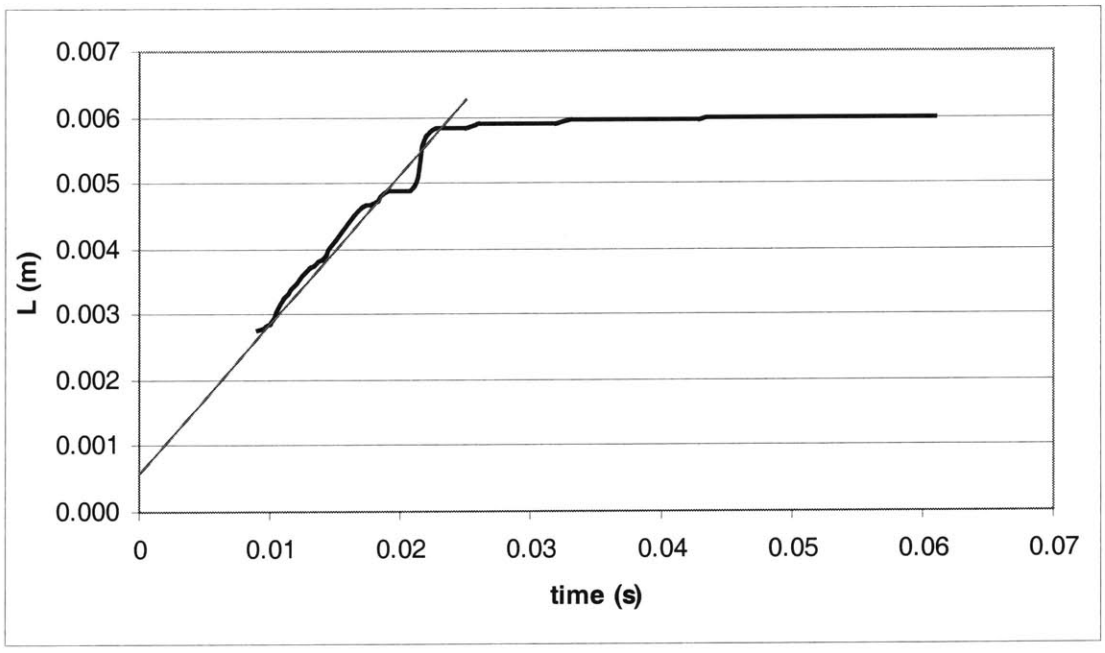

Figure 4.1.6 Drop deposited on an inclined plate ($\gamma = 45°$)
(Run 317 - S=0.43, also see Figure 4.1.2 (b)).
a) Top: Angle (deg.) versus time (s)
b) Bottom: Length of the drop L (m) versus time (s)

In the case of Figure 4.1.6 (b), the oscillations are also present and there is a possible partial arrest at time t = 0.02s. The average velocity during the fast spreading is 0.23m/s. Time zero has been adjusted so that the data would coincide with the extrapolation of L to zero with an average velocity of 0.3 m/s (see Figure 4.1.1), and therefore the line with a slope of 0.23m/s does not go through the origin.

From the comparison between these two cases, we note that though they have the same S and γ, they spread to distinctly different length. However, they both show an average velocity during their advance that is similar (see Figure 4.1.1); even though the best fit for run 317 is actually a little smaller (0.23m/s versus 3m/s) the difference is not large. They also both show two angles ($\theta_b \neq \theta_a$) with an approximate difference between them of 80° during the advance of the contact line, and this difference will tend to disappear as the drop is reaching equilibrium.

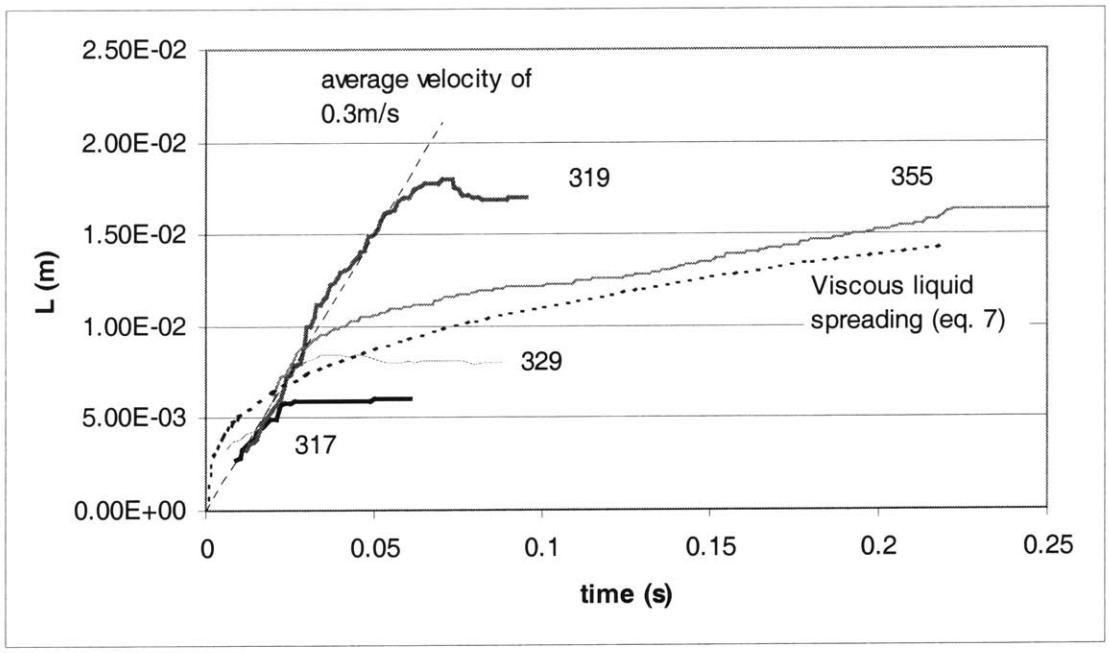

Figure 4.1.7 – Length of the drop as a function of time for four depositions at γ=45°

Figure 4.1.7 shows four different depositions on a plate inclined at $\gamma = 45°$ as well as the equation derived by Hocking (1990) describing a viscous fluid sheet going down an incline. The equation was transformed to our notations and following the assumption that the fluid is infinitely wide and has a cross-sectional area a^2 (2D flow model),

$$L = \left(\frac{9}{4} \frac{\rho g a^4 \sin\gamma}{\mu} t \right)^{1/3}. \qquad (7)$$

The four runs are the two cases mentioned above (run 317 and 319, both with S=0.43) as well as two others: run 355 (with S=0.08), and run 329 (with S=0.31). From this figure one can easily observe the large scatter in the parts where the molten contact line starts to slow down, and the fact that it does not appear to be dependant on S. However that may be, the observations made earlier regarding runs 319 and 317 (based on Figure 4.1.1) apply here as well. All depositions have two main stages of their advance, a first stage where the average velocity appears to be approximately constant for the four cases, and a second stage that corresponds to their deceleration and final arrest. The point at which they diverge from the first stage appears however to be random, and consequently their final length can vary by as much as a factor of five as can be observed from Figure 4.1.10. We also note from Figure 4.1.7 that the 2D viscous fluid sheet equation approximates fairly well the behavior of run 355 (S=0.08) from time t=0.025s to the arrest of the drop at t=0.25s

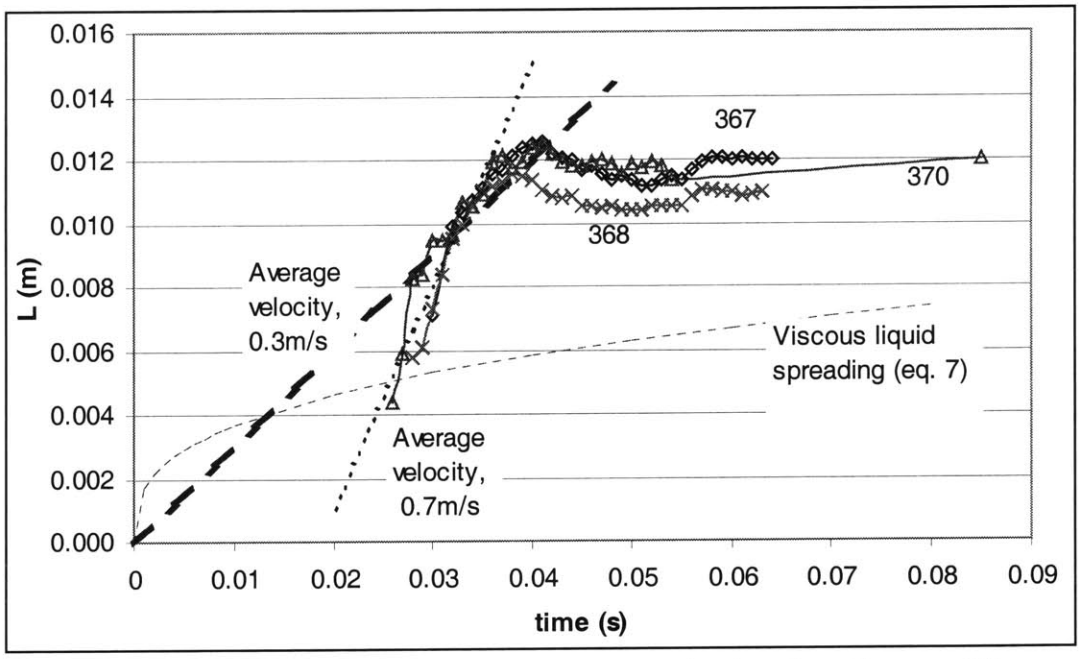

Figure 4.1.8 – Length of the drop as a function of time for three depositions at γ=15°

Figure 4.1.8 is similar to Figure 4.1.7 but for a small inclination angle of $\gamma = 15°$. We note that in this case also there is some data scatter, though much less than for $\gamma = 45°$ (see Figure 4.1.10). The three cases presented here are run 367 (with S=0.19), run 368 (with S=0.24) and run 370 (with S=0.42). It is apparent here also that the final length and break off from a constant average velocity are not primarily sensitive to S, but also, since

we do not have a deposition at $\gamma = 15°$ with a very low S, such as in the case of $\gamma = 45°$ (run 355, S=0.08), we cannot verify that the equation for the viscous liquid spreading (equation 7) would be a fair approximate. The two stages described for $\gamma = 45°$ are present here also. In Figure 4.1.8, we show two different "average" velocities. The first one has a value of 0.3m/s, the same as the one obtained for $\gamma = 45°$, while the second has a value of 0.7m/s and appears to be a rough approximation for the earlier period, shortly after impact. Though we have no compelling explanation for the higher average velocity in the early period (2-3 times larger than for spreading on a plate inclined at an angle of 45°) but presume that it is a result of the impact dynamics.

For an order of magnitude estimate, we can look at the spreading of a drop as a viscous flow going down an inclined plate (Fay (1994)). The shear stress forces will balance the gravity forces (Figure 4.1.9) and the Navier-Stokes equation (for the steady state case and with $\partial P / \partial x = 0$ since the air pressure is constant) will yield,

$$\frac{d^2u}{dy^2} = -\frac{\rho g \sin\gamma}{\mu} \tag{8}$$

which, with the no-slip boundary condition at y = 0, and shear stress at the free surface (y = h) equal to zero, gives a velocity profile u(y),

$$u(y) = \frac{\rho g \sin\gamma}{\mu}\left(hy - \frac{y^2}{2}\right) \tag{9}$$

and the velocity at the free surface (or maximum velocity) is equal to,

$$u(h) = \frac{\rho g h^2 \sin\gamma}{2\mu} \tag{10}$$

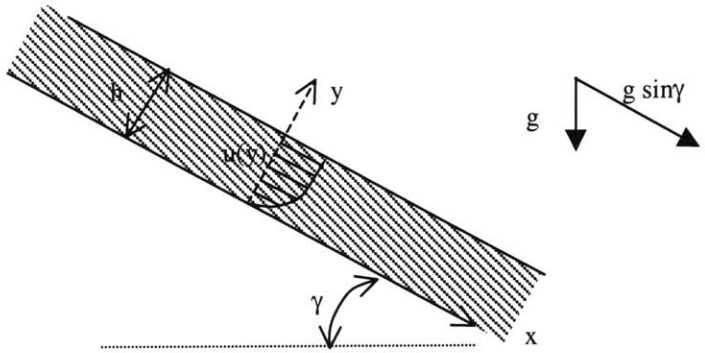

Figures 4.1.9 – Schematic of a flow down an inclined plane

An approximation of h, in our case, for the back of the head of the drop and beginning of the tail (region where the surface tension will play a lesser role), gives values from 1.5 to 0.7 mm, which in turns yields velocities in between 1.23 and 0.26 m/s. This approximation does not take in account the capillarity effect, the solidification, the impact oscillations, the inertia of the bulk of the drop, however it shows that the average velocity measured are in an acceptable order of magnitude.

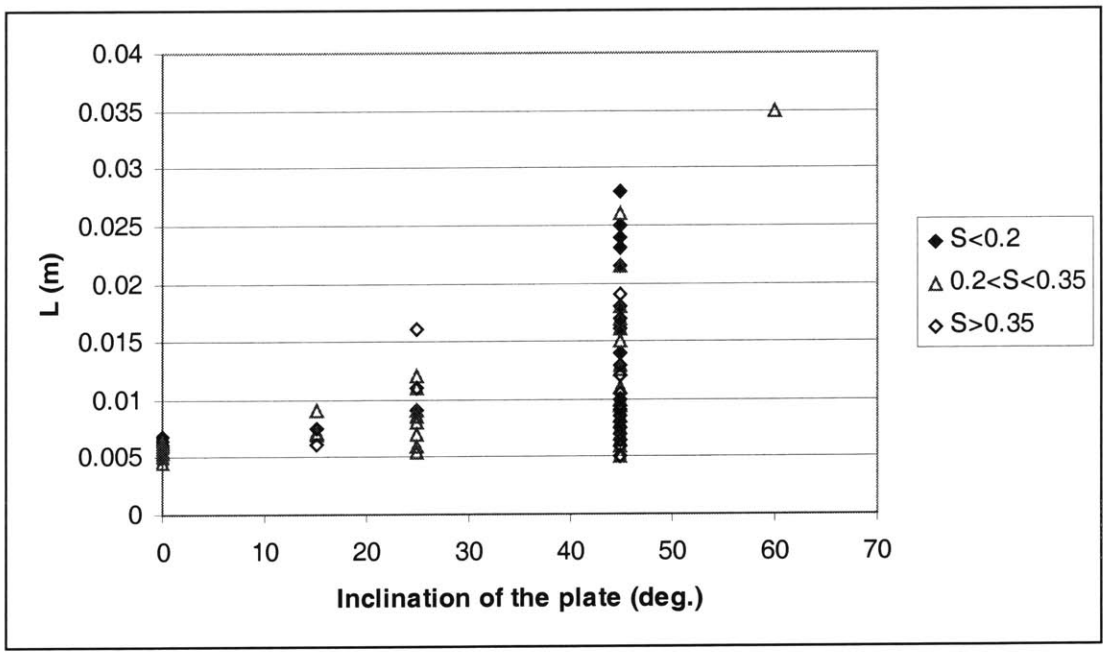

Figure 4.1.10 – Final length of all the drops deposited as a function of the inclination angle (γ).

We note from Figure 4.1.10 that this scatter of the data is especially important as the inclination of the plate increases.

Inclination angle (deg.), γ	Final length scatter
45°	5-28 mm
25°	5-16 mm
15°	6.2-9 mm
0°	4.5-6.8 mm

Table 4.1.1 – Summary of the scatter of the length as a function of the inclination angle γ.

Table 4.1.1 is a summary of Figure 4.1.10 and appears to be consistent with common observations of molten wax trickling down the side of a candle, where the final length of the drop also seems to be a non-repeatable phenomenon.

The fact that at γ=0° and γ=15° the data seem to be more repeatable may indicate that at high-inclination angles the non-repeatability comes from a non-equilibrium between the driving and resistive forces present, such that a small perturbation can greatly affect the final length of the spreading. In the case of γ=0° the temperature appears to be the primary factor. The shape of the drop and its angle of arrest were found to depend principally on S in previous work (Schiaffino and Sonin, 1997, and Duthaler, 1999). In the case of very low S, the inertia, capillarity and gravitational forces, as well as the angle of the inclination, should all be important factors. The solidification will, in this case, be very slow and should therefore play a role only in the final stages, possibly even (in the case of very low S) after the drop has reach mechanical arrest. The drop would in that case behave similarly to a simple viscous liquid going down a plate, with one difference: its tail is frozen, stuck to the plate (see consistency of the data of run 355 with equation 7, Figure 4.1.7). Capillarity forces, inertia, gravity, viscous resistance, and solidification are the main factors that control the molten contact line phenomenon. However, the fact that the conventional theory does not permit a prediction of the solidification near the contact line, due to the heat transfer singularity, limits our ability to formulate the problem mathematically and predict the shape.

From Figure 4.1.10, it also appears that the lower limit of the scatter is almost independent of the inclination (as well as S), while the upper limit of the scatter seems to be proportional to the angle of inclination.

It should also be noted that the drop experiences strong oscillations during its descent along the glass plate, which is a direct result of its impact on the plate. This may influence the dynamics of the drop's descent. Once the drop has reached its final length, the oscillations are still present and may affect the final approach to a static state. It also seems that these oscillations can be in or out of phase with the natural frequencies of the drop, making the damping of these oscillations longer or shorter, and thus influencing the final result in a complex way.

Also, the Stefan number will influence the final length, as well as the general shape of the drop. When S is low (high target temperature) the liquid will have a tendency to spread more laterally after impact, since the contact line does not freeze as readily, and consequently its trace will be wider, which influences the maximum length it can reach.

Another thing that also might increase the scatter observed is measurement errors. The picture are blurry due to motion which might make it difficult to distinguish between the two angles, θ_a and θ_b. From Figure 4.1.5 (a), we see that there are a few times during the descent of the drop where the region that defined θ_a was so small (or the picture was so blurry) that it was difficult to distinguish θ_a from θ_b. At these points (t=0.03s, 0.052s, 0.063s, and 0.078s) the two angles seemed to coincide, whereas they may not have. It is possible thereafter that the indicated jump of θ_a of 80° at these times are false.

There are many small factors that could have influenced the results, such as a contamination of the glass plate, dust particles, a change of humidity in the laboratory facilities, etc. As mention earlier, if the driving forces (gravity, inertia, capillarity) and retarding forces (viscosity, capillarity, solidification) are held in a precarious balance during the deposition and spreading of the molten contact line, small uncontrollable differences are in a position to make a big difference to the event.

4.2- Presentation of the data and comparison with previous work:

4.2.1- Post-solidification molten contact line arrest angles (the static angle):

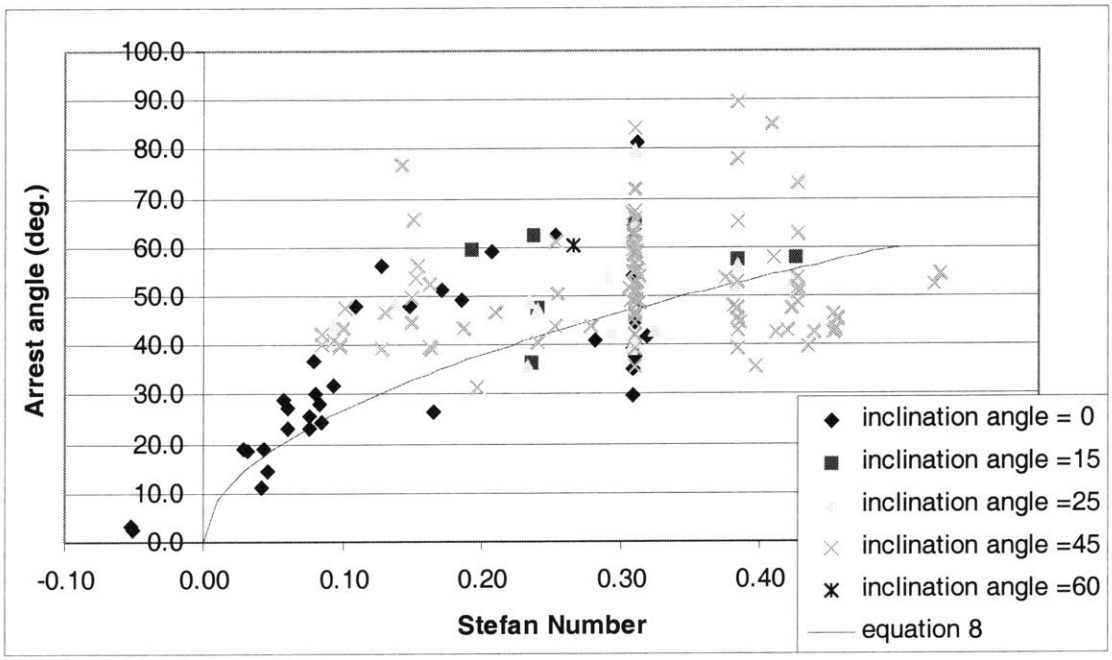

Figure 4.2.1.1 Post-solidification angle $(\theta_a)_\infty$ versus S.

Figure 4.2.1.1 shows all the post-solidification molten contact line arrest angles $(\theta_a)_\infty$ reported in appendix A, plotted against the Stefan number S (equation 5). The post-solidification angles $(\theta_a)_\infty$ are measured once the drop has reached its final solidified shape. The data are identified according to the value of the plate inclination angle (γ = 0°, 15°, 25°, 45° and 60°). The crucible temperature was T_o=90°C in all cases, so that both the ratio of liquid superheat to target sub-cooling β, and the Stefan number varied as the temperature of the target was varied.

$$\beta \equiv \frac{T_o - T_f}{T_f - T_t}, \qquad (11)$$

with T_f the fusion temperature (61.4°C for octocosane), and T_t the target temperature. A range of target temperature from 33 to 59°C was covered in the experiments, which corresponds to a range of β from approximately 1 to12, and a range of S from 0.03 to 0.4. High target temperatures (57°C and above) created experimental difficulties since the

melting temperature of octocosane is 61.4°C and the heater of the target overshot the set point temperature by a few degrees before adjusting to the set temperature. If this happened, it caused the melting of every previous deposition done on the same glass plate.

To minimize the oscillations of the drops, which we believe to be linked to the repeatability problem, the deposition at $\gamma = 0°$ (horizontal plate) were done differently: with the crucible close to the surface so that the drop formed around the tip of the crucible while touching the glass plate. The idea was to initiate melt contact and cause an outwardly spreading melt contact line over the target surface without inducing dynamic oscillations, and thus reduce the possibility of scatter due to oscillations (Figure 4.2.1.2). It appears from previous work (Schiaffino, 1996 and Duthaler, 1999) that the general shape of the drop should not affect the post-solidification contact angle, and therefore that the final angle should be the same regardless of how the spreading is initiated, if S and β are the same. This technique, however, could not be used for inclined plates since the inclination of the plate prevented the tip of the crucible from being close enough to the glass surface for the drop to stay attached. We had to keep in mind also that the temperature distribution in the melted octocosane could be affected, and also, to some extent, the temperature of the surface of the target. Some experiments were carried out, using thermocouples placed at different positions on the glass surface, to check the effects of the proximity of the crucible tip to the target. The results showed that after 2 to 3 minutes (upper limit on the time it would take to get spreading measurements), the surface temperature was not affected by more than 2-3°C when the tip of the crucible was at a height, h, approximately equal to 1 mm (run 256 in the appendix A). We were still careful when running these experiments to measure the angle and slowly pull away the crucible before it could affect the temperature of the target by more than ±1°C (runs 283 to 302 in appendix A).

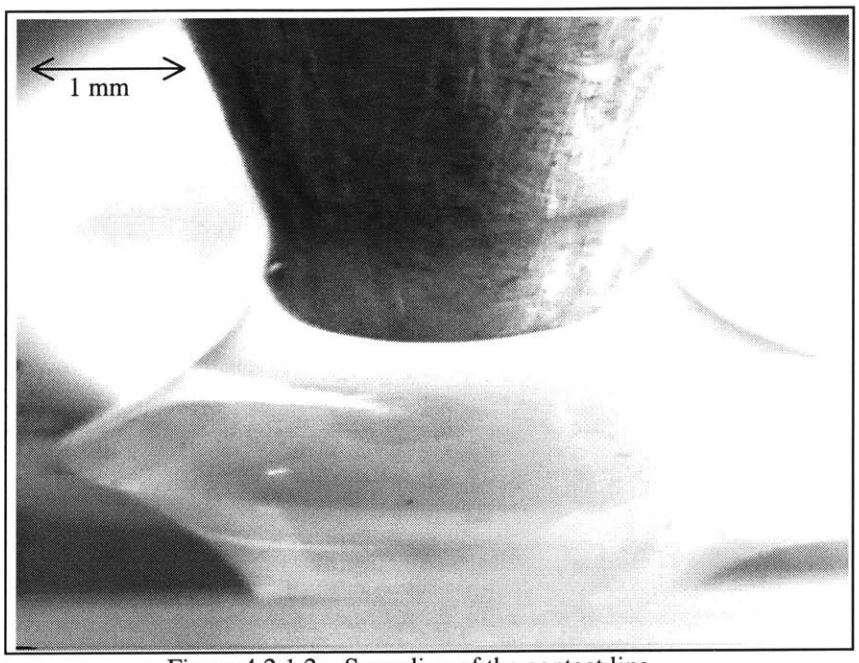

Figure 4.2.1.2 – Spreading of the contact line.
Picture taken with a CCD camera of run 292 ($\gamma = 0°$, S=0.03, β=12).

We noted, however, that at high Stefan number (low target temperature) the octocosane wets the surface of the target and solidifies very fast, at a time where the top of the drop is still attached to the tip of the crucible. As a result, the flow of molten material that is still coming out of the crucible is directed up along the crucible's exterior walls, along its tip, forming a pear-shaped drop. Figure 4.2.1.3 represents an extreme case with the crucible tip very close to the target so that this effect could be observed on camera. In this case, outward spreading of the melt onto the cold target is not achieved and the shape of the drop will be affected dramatically, as well as possibly the angle of contact with the plate. In cases where we let the drop fall from a distance of approximately 1 cm (the typical technique for deposition on an incline plate, see Figure 3.1) or when S was smaller (Figure 4.2.1.2), the melt flow was not blocked early in the experiment and contact line motion could be more readily studied. However that may be, the arrest angle obtained for $\gamma = 0°$, using the spreading or normal deposition techniques, seemed to agree roughly with the experimental results obtained by Schiaffino and Sonin (1997), and Duthaler (1999) despite the difference in the material used.

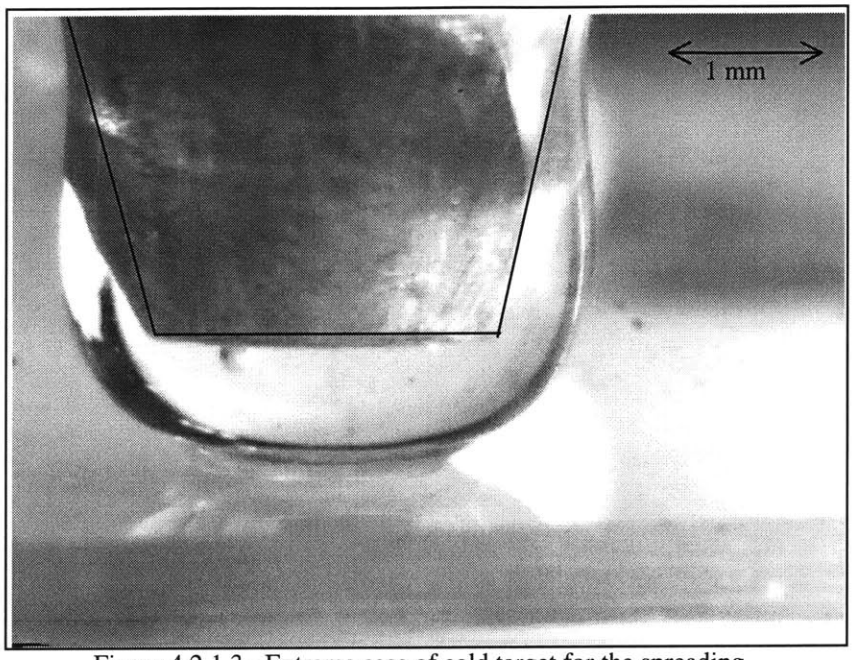

Figure 4.2.1.3 - Extreme case of cold target for the spreading.
Picture taken with a CCD camera ($\gamma = 0°$, S=0.35, β=1.2).
The black lines are an approximate limit of the crucible walls.
The molten contact line froze blocking the flow and forcing it along the walls of the crucible.

The continuous line In Figure 4.2.1.1 represents the equation that Schiaffino and Sonin (1997) obtained empirically for deposition of microcrystalline wax drops on a horizontal surface of the same material.

$$\theta_a = 85S^{0.5} \quad \text{degrees.} \qquad (12)$$

Disregarding the data scatter this equation is a fair approximation for all of our results regardless of the angle of the plate (γ), despite the fact that our data are a different molten material (octocosane versus microcrystalline wax), and despite the fact that our data are depositions on glass where theirs were depositions on the same material (on solid microcrystalline wax). A power law curve fit with Excel of our data for $\gamma = 0°$ (horizontal plate) yielded:

$$\theta_a = 84S^{0.44} \quad \text{degrees.} \qquad (13)$$

Considering that the angles are accurate to ±3° and the temperature to ±0.5°C, this is about the same as equation 8. This shows that the apparent contact angle at arrest, in the case of deposition on a horizontal plate, is controlled by S and therefore by the temperature difference, just as in the previous work done in this laboratory.

Similarly, if we take all the data with positive S, including all plate inclinations, and curve fit them on Excel with a power function, we obtain

$$\theta_a = 76S^{0.34} \text{ degrees.} \qquad (14)$$

These results suggest that the empirical equation derived by Schiaffino and Sonin (1997) may be applicable approximately to a broader range of materials similar to microcrystalline wax and octocosane, perhaps even to most waxes and paraffin.

4.2.2 The dynamics of the contact line:

Based on the dimensional analysis done by Schiaffino and Sonin (1997) on molten drop deposition at low Weber numbers, we can calculate a time scale of the spreading of the molten material onto the cold solid surface. Our drop depositions fall roughly into Schiaffino and Sonin's (1997) region II, where the characteristic spreading time is

$$\tau = \sqrt{\frac{\rho a^3}{\sigma}}, \qquad (15)$$

For our range of values of a (1.5 - 2 mm), τ = 0.01 - 0.015s. Table 4.2.2.1 shows these values as well as the thermal diffusion time scale,

$$\tau_{ther} = \frac{a^2}{\alpha}, \qquad (16)$$

and the drop's volume, V_o.

Radius of the drop, a	2.00E-03	m	1.50E-03
Volume, V_o	3.35E-08	m^3	1.41E-08
Spreading time scale	1.54E-02	s	1.00E-02
Thermal diffusion time scale	50.96	s	28.66

Table 4.2.2.1 – Range of the parameter values in experiments.

Schiaffino and Sonin (1997) obtained an empirical fitting formula for the contact line diameter as a function of time, for deposition on a flat plate in region II of their empirical conditions. This formula applies to the limit $\theta_e \to 0$ (where θ_e is the equilibrium angle as found in the Young's equation, equation 1) in isothermal liquid deposition, or for $S \to 0$ in the case of melt deposition on the same solid, as well as for $S>0$ prior to contact line arrest. The formula is

$$\frac{D}{a} = 4.8\left[1 - \exp\left(-0.9\frac{t}{\tau}\right)\right], \qquad (17)$$

where D is the diameter of the drop's contact line during spreading, a is the radius of the molten drop before deposition, t is the time, and τ is given by equation 15.

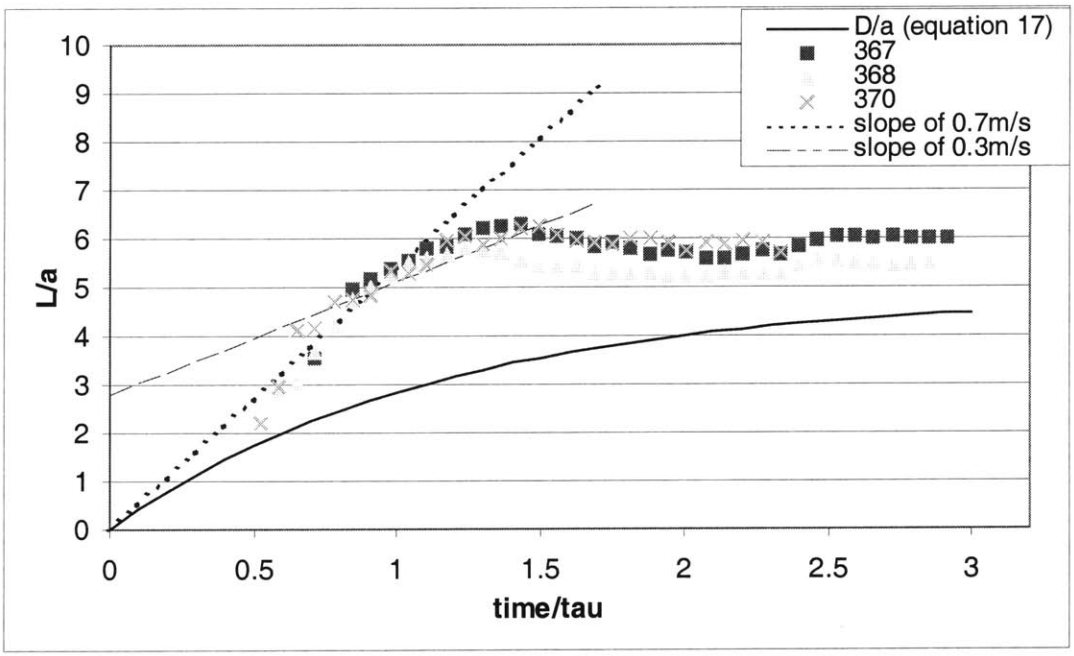

Figure 4.2.2.1 – Length of three drops (L/a) as a function of time (t/τ_{osc}).
All three runs at γ=15° with different values of S: 0.19, 0.24 and 0.43 respectively.
The continuous line is equation 13, the correlation derived for low We deposition on a flat plate by Schiaffino and Sonin (1997).
The dashed lines are the constant average velocities as discussed in section 4.1.

The correlation for flat plate does not fit exactly the data for deposition at γ=15°, as was expected, because the melt shape was oblong rather than circular (see Figure 4.2.2.2), and the impact Weber number, while not large, was not very small either (see Schiaffino and Sonin, 1997). If instead of L we were to report the ratio of the length to the thickness of the drop as it evolves down the plate in time, the relation would have

been closer to fit the correlation for the diameter. Indeed, the ratio (measured after the drop solidified) of the drop length to its width is approximately 1.5 (Figure 4.2.2.2), which if multiplying the theoretical curve would put it slightly above the data presented in Figure 4.2.2.1.

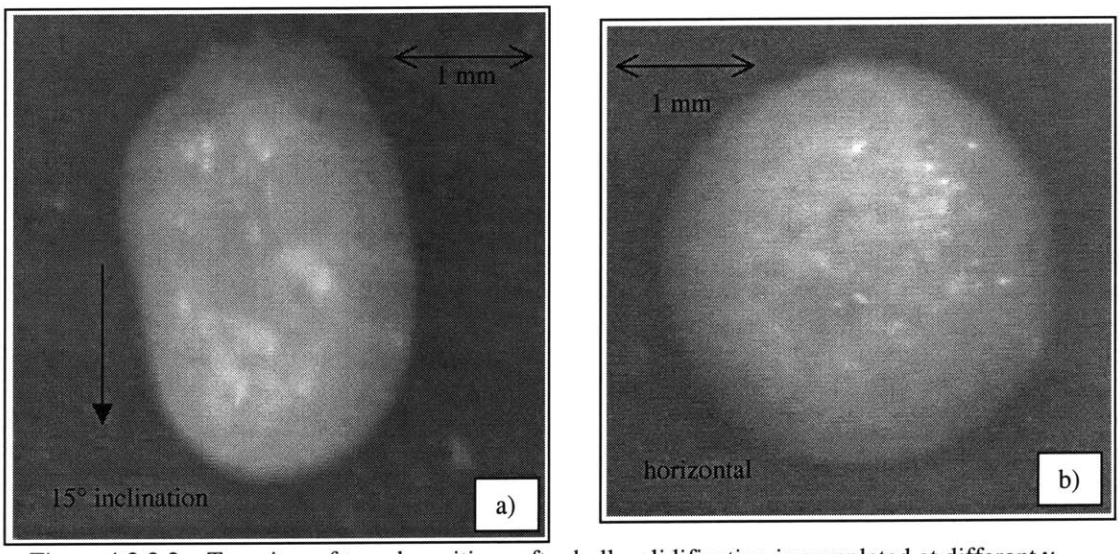

Figure 4.2.2.2 – Top view of two depositions after bulk solidification is completed at different γ.
(a) γ=15° (Run 368)
(b) γ=0° (Run 177)
(the arrow shows the direction of the motion, i.e. the downward direction along the plate)

From successive frames of the spreading drop, we can calculate an instantaneous velocity, and from each frame we obtained the angles θ_a and θ_b, which can be presented as functions of the capillary number Ca, the non-dimensional velocity, equation 3. Such a plot is shown in Figure 4.2.2.3 for $\gamma = 45°$ and various values of the Stefan number S.

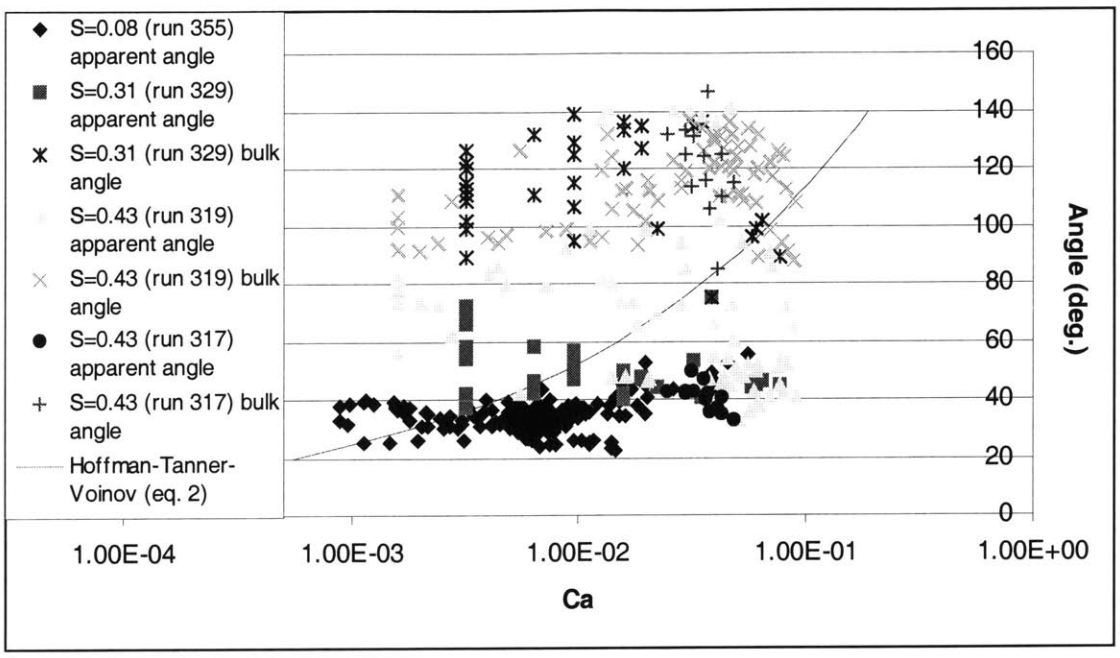

Figure 4.2.2.3 – Angle (deg.) as a function of Ca for drop deposited on plate with $\gamma = 45°$
The continuous line is equation 2, the Hoffman-Tanner-Voinov law is the special case of $\theta_m=\theta_e=0°$

In three out of the four runs presented in Figure 4.2.2.3 (runs 329, 319, and 317), the drops have both angles θ_a and θ_b (that is $\theta_a \neq \theta_b$). θ_a is represented with solid data points, and θ_b with crosses. The Hoffman-Tanner-Voinov law, equation 2, is shown as a continuous line, with $\theta_m = \theta_e = 0°$, which is the form of this equation that Schiaffino and Sonin (1997) showed would fit the molten contact line data for deposition of microcrystalline wax droplets on a cold, horizontal surface of the same material. Duthaler (1999) developed another law referred to as the near-arrest law limit, where θ_a approaches the value of θ_s (see Figure 4.1.4).

The scatter in Figure 4.2.2.3 is so large, however, that it is difficult to contemplate deducing a function $Ca=f(\theta_a,\theta_b)$ or $Ca=f(\theta_a)$ from the data. Even if we ignore the bulk angle θ_b (considering it a dependant variable) and seek only a relationship between θ_a and Ca, as was done by Schiaffino and Sonin (1997) and Duthaler (1999), there is too much scatter in the data (run 319 for example). The data which seem to be the best behaved are the ones of run 355, where S=0.08, in which case the target temperature was only slightly below the melting point, making the molten contact line spread much like a viscous fluid down an inclined plate without much influence from solidification except for the pinning of the tail to the plate and the eventual arrest of the advancing contact line.

In some cases the drop does not have two angles, that is $\theta_a = \theta_b$. This happens at low Stefan number (S=0.08 – run 355) or at small inclination of the plate ($\gamma = 15°$). We have $\theta_a = \theta_b$ in the cases with less scatter, and $\theta_a \neq \theta_b$ when there is a lot of scatter, indicating that the driving and resistive forces are in a precarious balance. In most cases presented here, however, we have $\theta_a \neq \theta_b$, which corresponds to an average temperature (T_t = 25-50; S = 0.16-0.5; β = 0.8-2.51), and an average inclination angle (γ = 25-50). The drop's shape and behavior is more complicated to predict than the one previously studied of deposition on a cold flat plate of the same material (Gao and Sonin, 1994, Schiaffino and Sonin, 1997, and Duthaler, 1999).

4.2.3 - The Stick-slip behavior (near-arrest behavior):

"Stick-slip motion" of molten contact lines was noted first by Duthaler (1999) at low Stefan number on an inclined plate. Duthaler's observations suggested that the drop's contact line would momentarily arrest and then resume motion, thus experiencing oscillations in velocity during its descent. We note that oscillations in velocities are more easily noticed at low S because low S implies higher target temperature and therefore a longer time of spreading to observe such variations in velocity. This phenomenon may also happen at high S, but is then more difficult to observe.

The reason for "stick-slip motion" can be imagined by considering the wedge-like solidification front that starts right behind the advancing contact line (see Schiaffino and Sonin, 1997), as pictured in Figure 4.2.3.1 (a). If, due to liquid melt oscillations, the liquid contact angle is reduced so that it approaches the solid wedge angle, freezing of the contact line would occur. The flow could re-start by liquid inertia (see Figure 4.2.3.1 (b)), and/or by an increase of the heat flux due to the forward circulation of the molten liquid inside the drop, as first described by Gao (1994), resulting in a re-melting of the front.

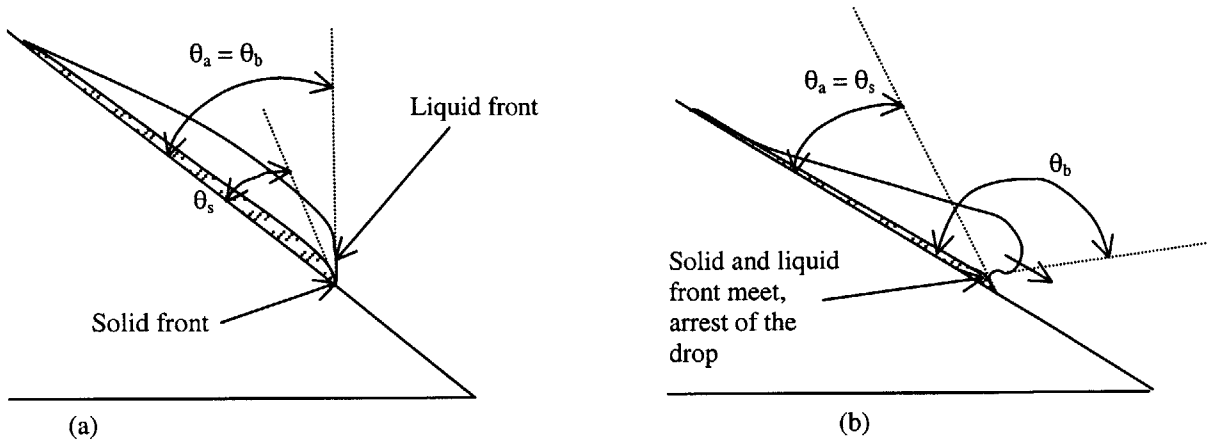

Figure 4.2.3.1 Schematic of the expected "stick-slip" behavior.
(a) The drop is advancing.
(b) It is arrested, but the liquid phase's inertia, represented by the arrow, is about to overcome the arrest.

This explanation of "stick-slip motion" is related to the explanation of the two angles θ_a and θ_b. "Stick-slip" could occur whenever θ_a approaches the solidification front angle θ_s causing arrest, whether temporary or final. Measuring θ_a, at arrest thus gives us an indication of θ_s.

Our resolution of the speed of the drop's front was, unfortunately, not sufficient to conclusively demonstrate that there was in fact "stick-slip motion" (see Figure 4.2.3.2 for the length as a function of time compared with the solidified trace of the drop showing possible arrests (run 319) as noted in the figure). However, there were also other indications that suggested that "stick-slip" behavior occurred. There are changes in the width of the trace left behind an advancing drop after solidification (Figure 4.2.3.2, 4.2.3.3, and 4.2.3.4). In several cases, the change in the width of the trace was accompanied by an observable change of melt thickness right before the change of width occurs, which could have been caused by a temporary arrest of the contact line and a "pile-up" of melt behind it due to liquid momentum. Unfortunately these observations also were not very repeatable. On one plate and under similar conditions, one can observe many different shapes and length of deposited drops (Figure 4.2.3.3).

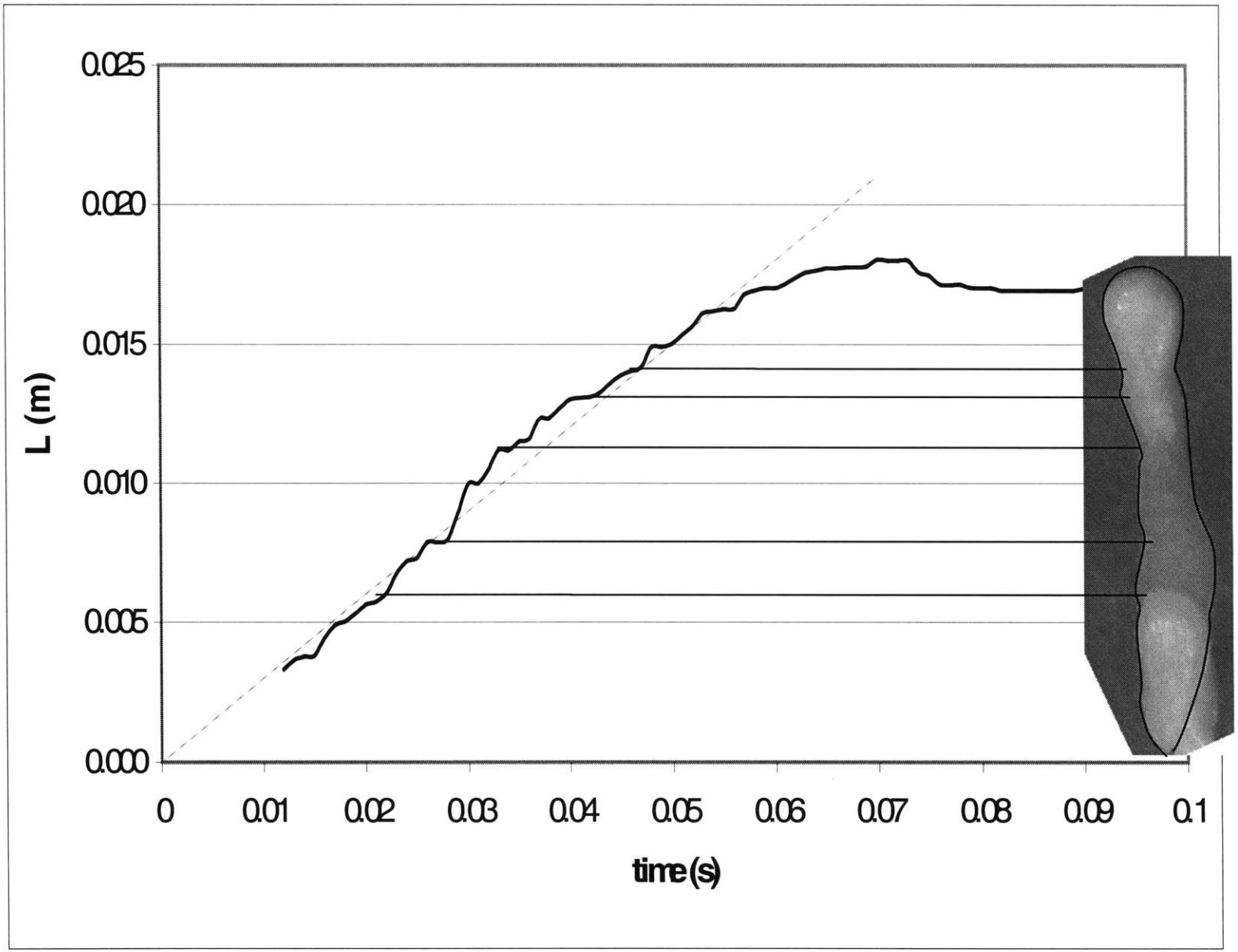

Figure 4.2.3.2 - Length L (m) as a function of time (s) for run 319 ($\gamma = 45°$, S=0.43), comparison with a top view of the drop after solidification.

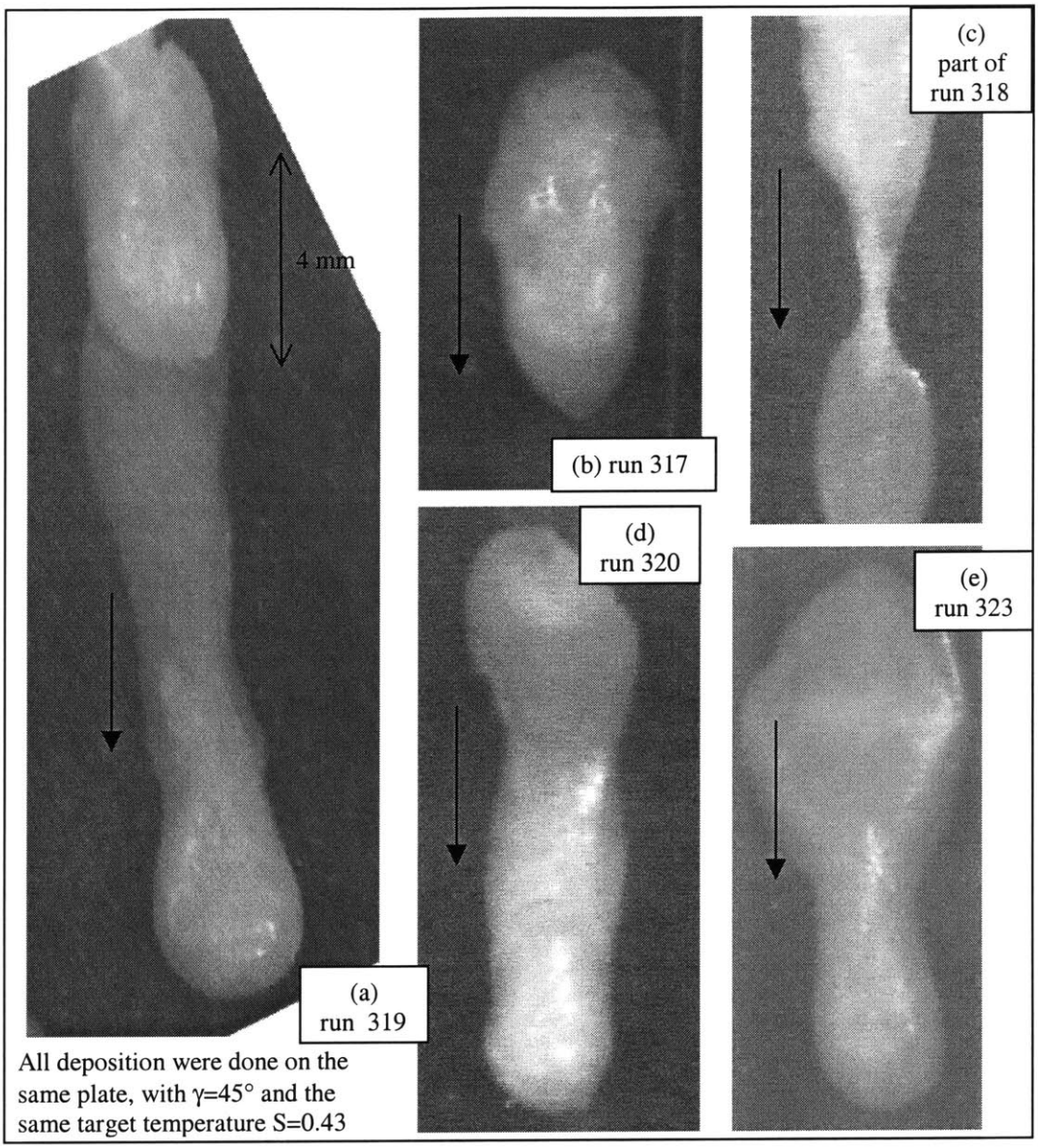

Figure 4.2.3.3 – Five pictures of top views of plate 27, all deposited under the same conditions: $\gamma=45°$, S=0.43.

- In picture (a) we have another deposition that happened on top of an already solidified drop, the drop that solidified on top was not taken in account since then we have an octocosane-octocosane spreading (instead of octocosane on glass).
- In picture (c), the width of the drop became a thread (less than 1 mm), before continuing spreading along the plate (possible proof of partial arrest/jump in velocity).

(the arrow shows the direction of the motion, i.e. the downward direction along the plate and all the pictures have the same scale)

However, from Figure 4.2.3.4 one can see that though the results do not appear repeatable, they show a pattern related to the temperature of the target and therefore to the value of S. For low S (higher target temperature) the drop's traces are wider and

thinner, therefore changes in width and thickness are more difficult to make out (Figure 4.2.3.4). At higher S, however, the changes in width are obvious, sometimes becoming a mere thread (less than one millimeter in width as in Figure 4.2.3.3 (c)), and so thin that they sometimes broke during the solidification process (octocosane shrinks during solidification). One can also observe that the higher the angle γ is (Figure 4.2.3.5), the less obvious the change of width is, probably due to a higher and more uniform velocity, much like an ordinary liquid flowing down a plane.

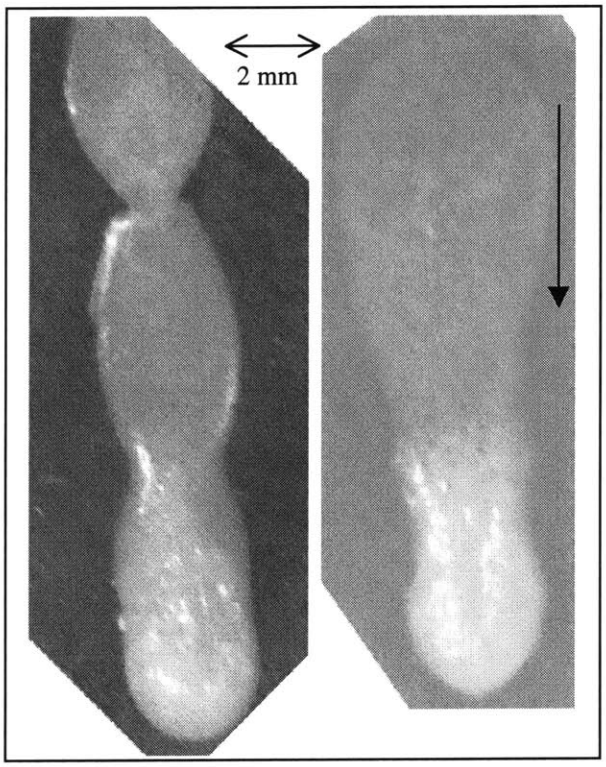

Figure 4.2.3.4 – (a) Top view of run 155, with γ=45°, S=0.31.
(b) Top view of run 346, with γ=45°, S=0.1
- The difference of width and thickness due to the change of S.
- In the left picture (a) the change of width (possible proof of a partial arrest/jump in velocity)
(the arrow shows the direction of the motion, i.e. the downward direction along the plate and all the pictures have the same scale)

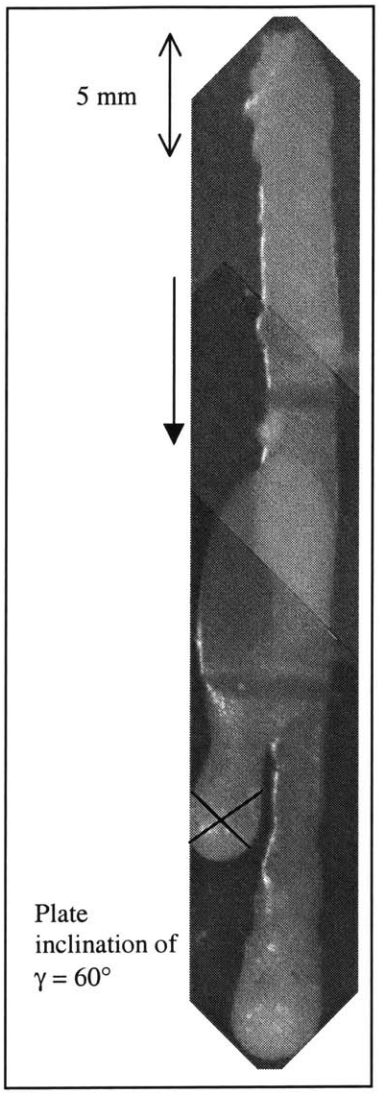

Figure 4.2.3.5 – Top view of run 369, with γ=60°, S=0.27.
- A second drop was deposited after solidification of the first drop.
(the arrow shows the direction of the motion, i.e. the downward direction along the plate)

These shapes may point to "stick-slip behavior" as discussed in connection with Figure 4.2.3.1. Some of the solidified drops have shapes similar to the one in Figure 4.2.3.1 (b), as if the inertia and circulation of the molten material did not achieve the breaking of the solidified front (Figure 4.2.3.6).

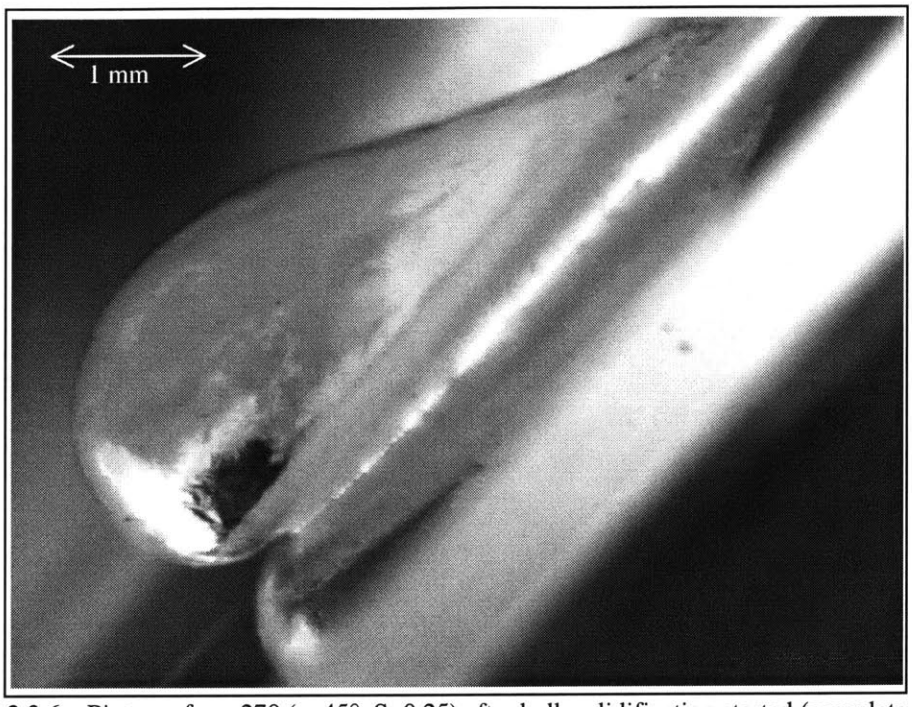

Figure 4.2.3.6 – Picture of run 270 (γ=45°, S=0.25) after bulk solidification started (complete arrest).

4.2.4 – Two other near arrest phenomena observed.

Spreading on an horizontal plates ($\gamma = 0°$) at low Stefan number sometimes showed a behavior similar to the "stick-slip motion" described above. It was noticed that the melt experiences bulk oscillations as it first spreads on the plate, and this leads to oscillations in contact line velocity. Torresola (1998) also mentioned this behavior with deposition of octocosane and suggested that it might be due to freezing and re-melting of the solidified front, that is, the same "stick-slip behavior" as observed on inclined plate. However, further experiments should be done to clarify the origin of this phenomenon.

For deposition on a plate inclined at a small angle (such as $\gamma = 15°$), it seems that the drop reaches its final arrest point, passes it, and then oscillates around this point, before settling into its final shape. These observations seem to be the consequence of dynamic oscillations, but could also involve or cause "stick-slip motion".

Once the drop touches the surface, it wets the surface of the glass while taking a dome shape as gravity pushes the liquid front down the incline. The drop extends and a dimple is created on top of it (Figure 4.2.4.1), which appears to be the effect forcing the

drop's contact line past its final arrest point. The creation of the dimple until its disappearance by rebound temporally stretches the drop until it retracts to the final arrest point.

The dimple's disappearance leads to the creation of a hump (dome shape) at the front of the drop that seems, in turn, to push the liquid front again past its final arrest and as the hump disappears takes the front back to its final arrest (Figure 4.2.4.1 and Figure 4.2.4.2).

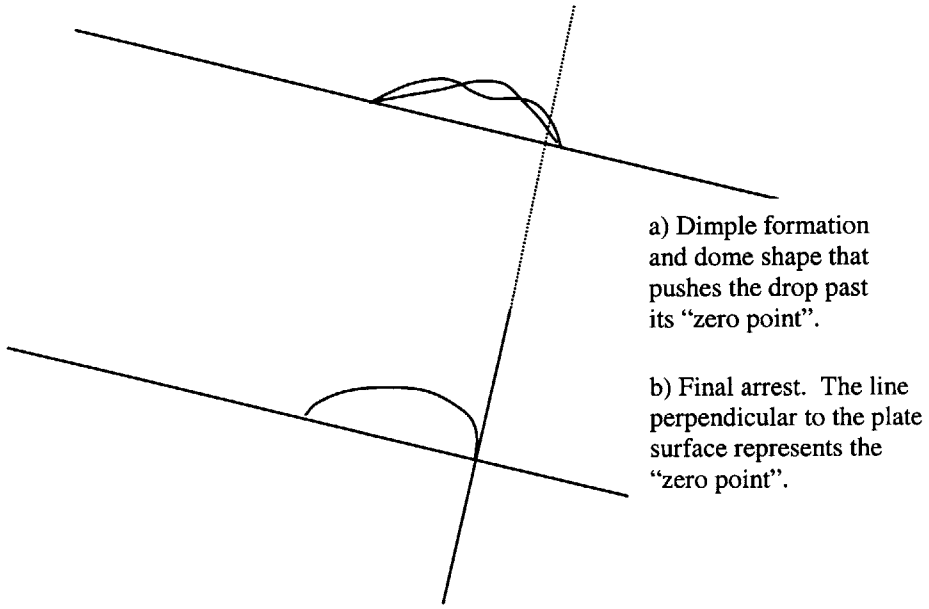

Figure 4.2.4.1 General shape observed in the case of spreading with strong oscillations on a cold solid surface inclined at γ=15°.

Figure 4.2.4.1 represents a sketch of the observed shapes taken by the drop. The first drawing (a) represents the two dynamic stages observed, while the second (b) is the shape after final arrest. Figure 4.2.4.2 shows a sequence of pictures of the liquid overflowing its final arrest point and retracting to it. The white arrows represent the final arrest point and the shapes are bounded with a white line to aid observations. The contact angle is reduced as the drop moves forward past its final arrest and increases again as it retracts towards it, as shown in Figure 4.2.4.3.

Figure 4.2.4.2 – Run 368 ($\gamma = 15°$, S= 0.24)
Spreading of a drop with strong oscillations on a cold solid surface inclined at γ=15°.

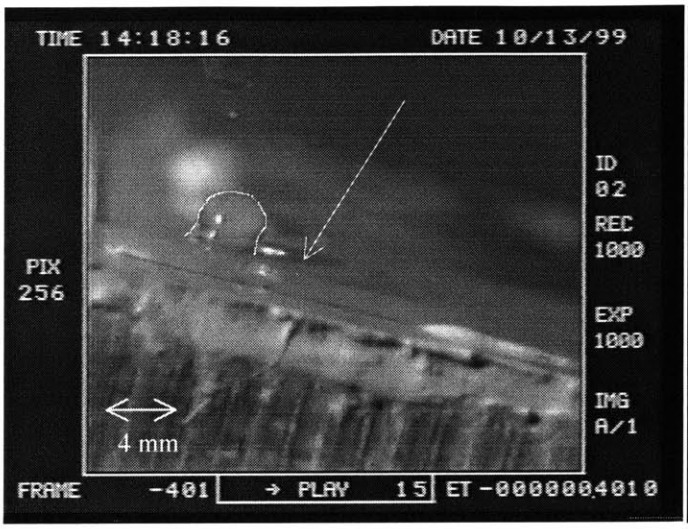

Initial shape of the droplet as it first touches the inclined plane.

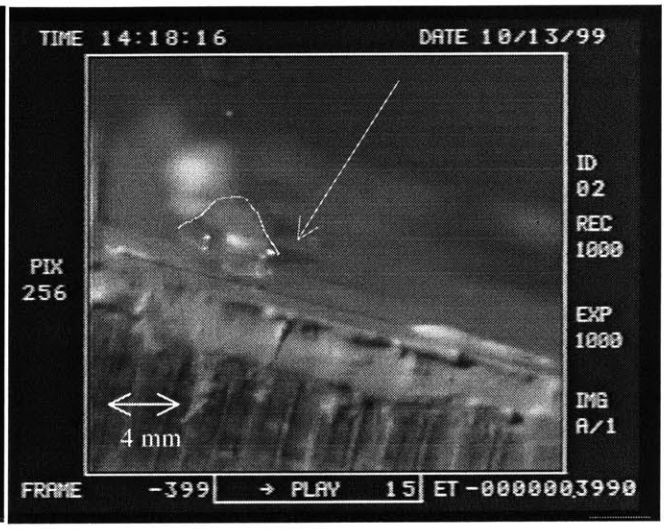

t=0.002s

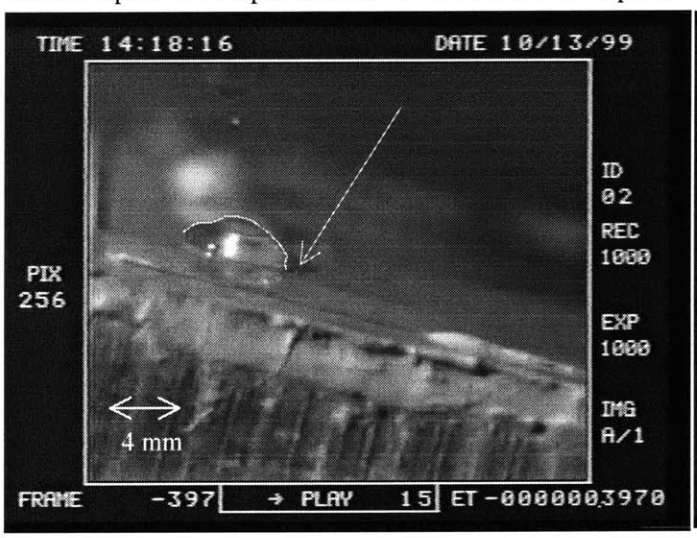

t=0.004s

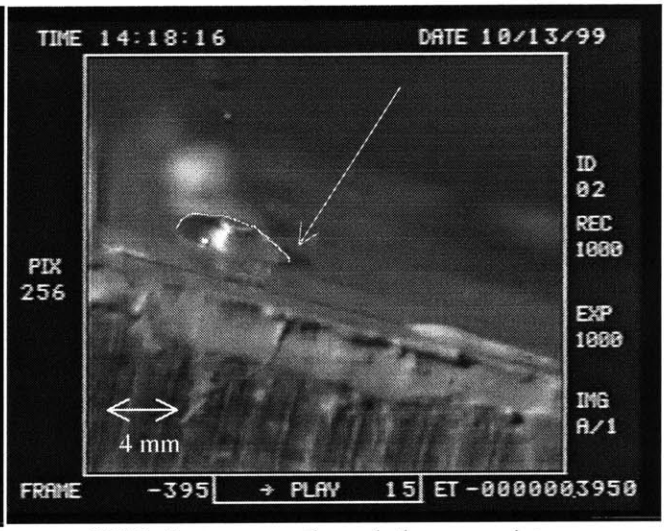

t=0.006s first passage through the zero point.

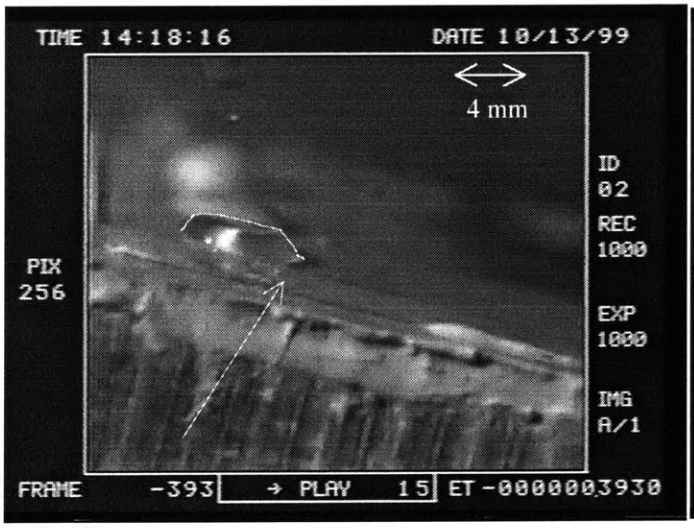

t=0.008s

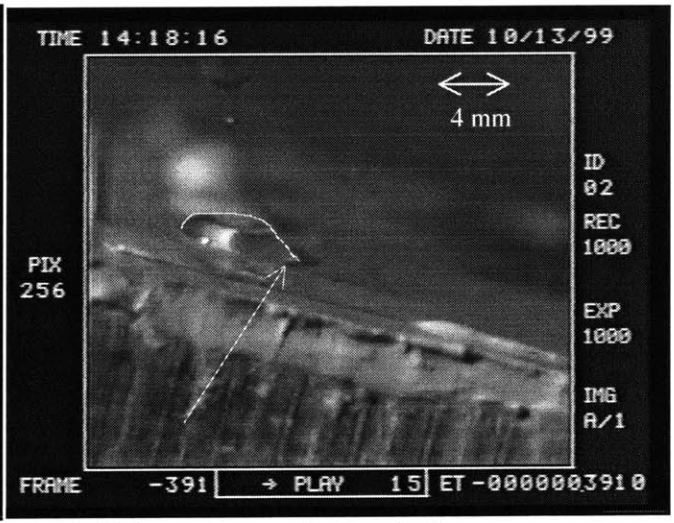

t=0.01s; maximum extent reached

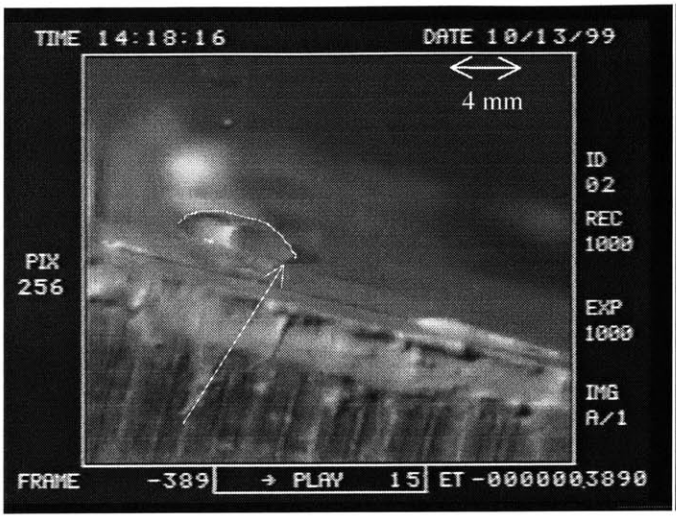

t=0.012

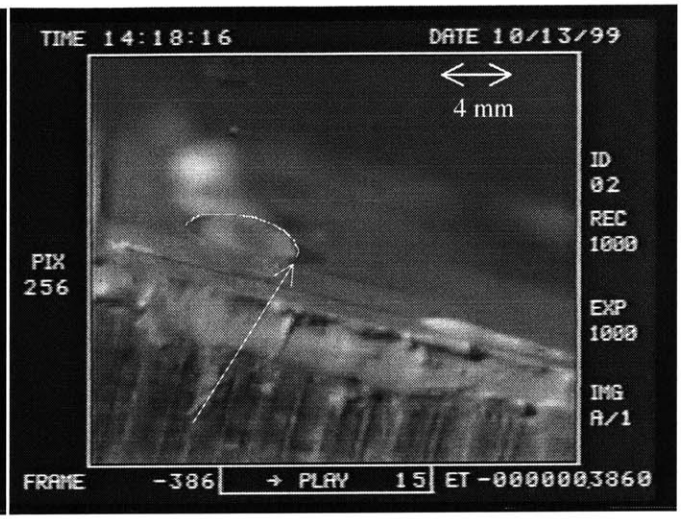

t=0.015s; passage through the zero point

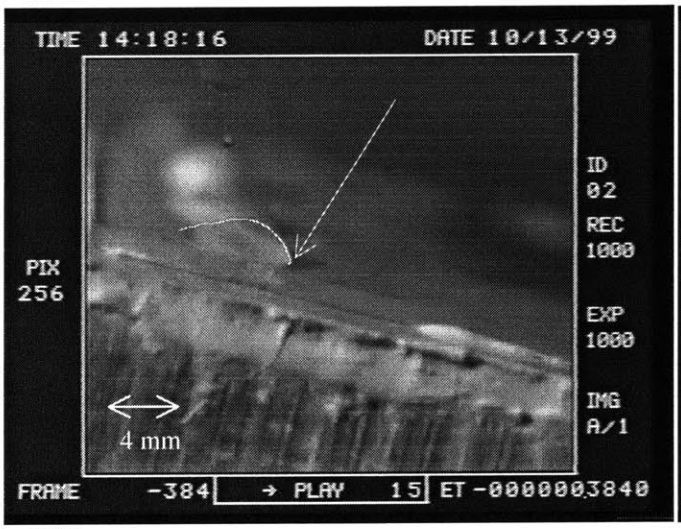

t=0.017s

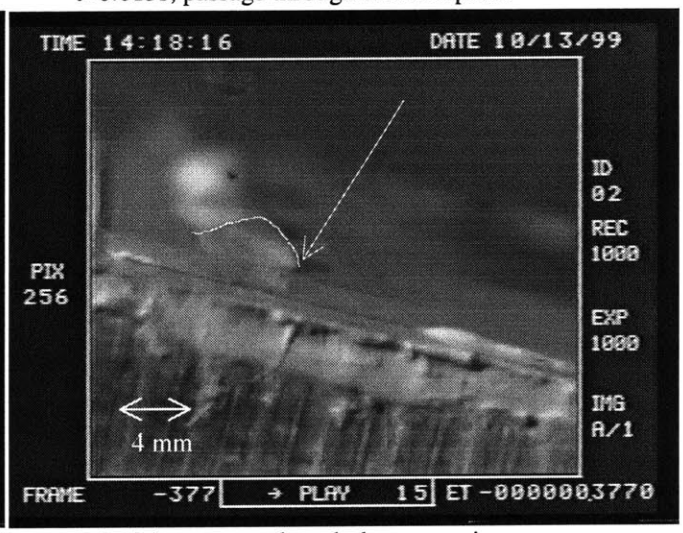

t=0.024s; passage though the zero point

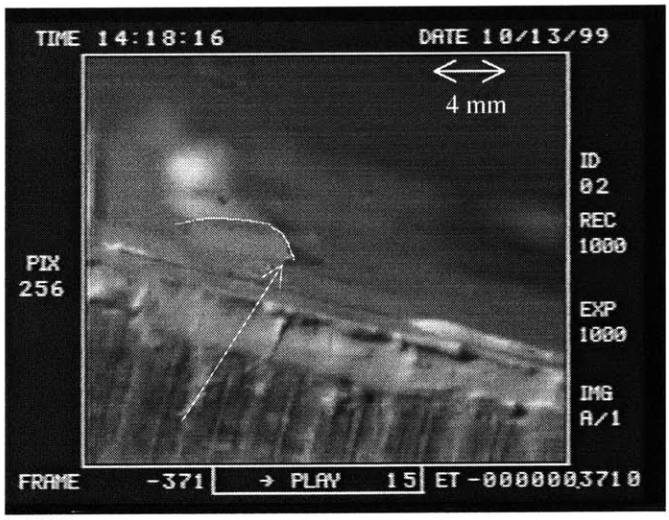

t=0.03s

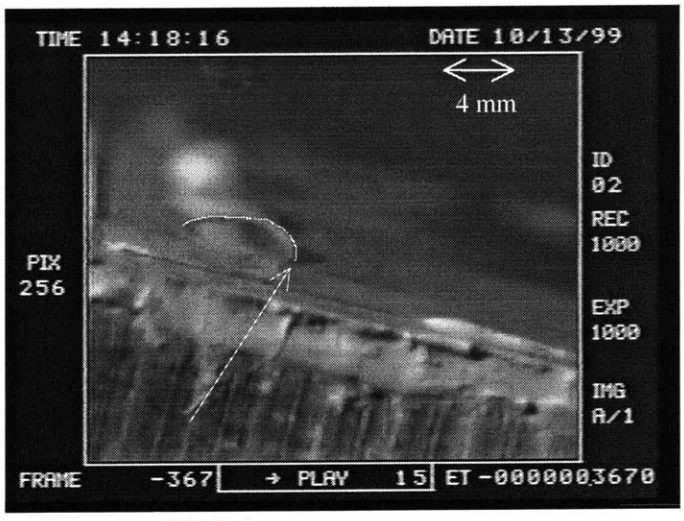

Final shape

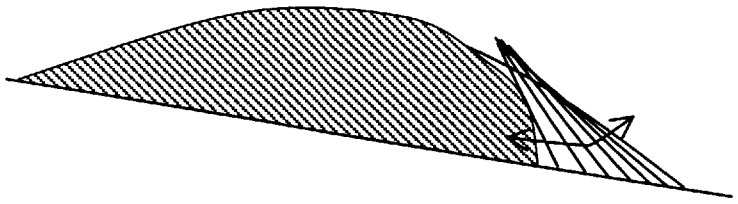

Figure 4.2.4.3 Evolution of the angle observed in the case of spreading with strong oscillations on a cold solid surface inclined at γ=15°.
The original shape and final shape is represented by the dashed pattern. The arrow indicates the advance and corresponding change of angle.

We note that once the surface is wetted, the contact may not be octocosane on glass anymore, but octocosane on octocosane if a thin filmed has been left behind by the retracting drop.

5 - Concluding remarks:

We have examined the deposition of molten octocosane drops on a cold glass surface at conditions such that $25°<\gamma<50°$, $0.16<S<0.5$, and $0.8<\beta<2.5$. Based on observations of 373 depositions, we conclude that the experiments suffered from significant scatter (lack of repeatability), despite apparently well controlled initial conditions. The greatest scatter occurred in the length of the deposit and the molten contact angle, i.e. in overall shape. However, data obtained in one of these two regions of the spreading condition defined by $\gamma \leq 15°$, or by $Tt \geq 50°C$ ($S \leq 0.15$, $\beta \geq 2.75$) was quite more reproducible.

We speculate that the repeatability problem is linked to a precarious balance between the driving (gravity, inertia, capillarity) and resistive (viscous, capillarity, solidification) forces involved in the spreading of the drop. Small random differences appear to cause large differences in the drop's shape and behavior.

We did note, however, some similarities between the runs. All run consist of two main stages. In the first stage the molten contact line advances with an approximately constant average velocity (in the range of 0.3m/s), and in the second the contact line decelerates and arrests. While both stages exist in all cases, the end of the constant velocity region appears to occur randomly and therefore the final length of the drop is not repeatable.

We also observed that some drops have shapes that can be described at times in terms of two angles. The first one is the bulk angle θ_b, which represents the contact angle extrapolated from the bulk of the liquid. This angle is affected by the drop's inertia. The second is the apparent angle θ_a, as observed close to the target's surface, at a distance of the order of 100 μm. The value of θ_a approaches the melt's solidification angle θ_s at the point where the contact line arrests. While not all drop depositions have these two angles, the ones that do tend to be the non-repeatable cases. We noted also that the two angles tend to become equal when the drop reaches a final equilibrium position.

We observed that drops deposited at very low S and drops deposited at a very small or zero inclination angle γ were the most repeatable ones. In fact, if a drop spreads at very low S (surface temperature close to the melting point) it will behave in a way

similar to a viscous liquid spreading along a plate (corresponding approximately to the isothermal case), the only difference being that its tail is pinned to the glass target surface due to solidification (Figure 4.1.7 and equation 7). If γ is small or zero (horizontal plate) then the drop will behave in a way similar to that described by Schiaffino and Sonin (1997) or Duthaler (1999). We then find that $(\theta_a)_\infty$ is a function of S (roughly following equation 12 or 13).

We also obtained some evidence of "stick-slip" behavior of the molten contact line, based in part on undulations in the deposition's width that appear to be related to oscillations of velocity. Some drops also appeared to have solidified while their bulk inertia was trying to overcome arrest. Though none of those observations conclusively proved the existence of a "stick-slip" behavior, two other related phenomena were observed primarily at low γ. These were oscillations of the length and of the velocity of the molten contact line on an horizontal plate. The present study reinforce the need for further investigation of near-arrest phenomena before a final conclusion can be drawn on the exact processes that take place during the spreading and contact line arrest.

Symbols

α	Thermal diffusivity (m^2/s)
β	Ratio of liquid superheat to target sub-cooling (eq. 11)
γ	Inclination angle of the target above the horizontal
κ_H	Proportionality coefficient in the Hoffman-Tanner-Voinov law (eq. 2)
μ	Absolute viscosity (Pa.s)
ν	Kinematic viscosity (m^2/s)
σ	Surface tension associated with the liquid/gas boundary (N/m)
σ_{sg}	Surface tension associated with the solid/gas boundary (N/m)
σ_{sl}	Surface tension associated with the solid/liquid boundary (N/m)
θ_a	Apparent contact angle
$(\theta_a)_\infty$	Post-solidification value of the apparent contact angle
θ_b	Bulk angle
θ_e	Equilibrium angle (eq. 1)
θ_m	Slope of the free surface ($\sim\theta_e$)
θ_s	Angle of the solidification front
ρ_s	Solid density (kg/m^3)
ρ_l	Liquid density (kg/m^3)
τ	Characteristic time scale (eq. 15)
τ_{ther}	Thermal diffusion time scale (eq. 16)
a	Radius of the liquid drop before impact (m)
Ca	Capillary number (eq. 3)
c_p	Specific heat (J/kg K)
D	Diameter of a drop in deposition on an horizontal plate (m)
g	Gravitational constant ($g=9.81\ m/s^2$)
h	Height of liquid (m)
h_{fg}	Latent heat (kJ/kg)
k	Thermal conductivity (W/m K)
L	Length of the drop (m)
r_b	Half extent of a drop (eq .4) (m)
S	Stefan number, (eq. 5)
t	Time (s)
T_f	Fusion temperature (°C)
T_o	Molten drop temperature (°C)
T_t	Target temperature (°C)
u(y)	Velocity profile (m/s)
U	Contact line velocity (m/s)
V_o	Volume of the drop (m^3)

Reference

Dussan V., E.B. 1979. On the Spreading of Liquids on Solid Surfaces: Static and Dynamic Contact Lines. *Ann. Rev. Fluid Mech.* **11**, 371-400.

Duthaler, G. 1999. Molten Drop Deposition and the Dynamics of the Molten Contact Line. Ph.D. Thesis, Department of Mechanical Engineering, MIT.

Fay, J.A. 1994. *Introduction to Fluid Mechanics*. MIT Press, Cambridge, MA.

Gao, F. 1994. Molten Microdrop Deposition and Solidification Processes, Ph.D. Thesis, Department of Mechanical Engineering, MIT.

Gao, F. & Sonin, A.A. 1994. Precise deposition of molten microdrops: the physics of digital microfabrication. *Proc. R. Soc. Lond.* A **444**, 533-554.

Goodwin, R. & Homsy G.M. 1990. Viscous flow down a slope in the vicinity of a contact line. *Phys. Fluids* **3** (4), 515-528.

Hocking, L. M., 1990. Spreading and instabilities of a viscous fluid sheet. *J. Fluid Mech.,* **211,** 373-392.

Hocking, L. M., 1992. Rival contact angle models and the spreading of drops. *J. Fluid Mech.,* **239**, 671-681.

Kistler, S.F. 1993. Hydrodynamics of Wetting. Wettability. *Surfactant Science Series* **49** (6), 311-429.

Quintella, M.A. 1999. Numerical Investigation of the Heat Flux Singularity at an Advancing Molten Contact Line. MS thesis, MIT.

Schiaffino, S. 1996. The Fundamentals of Molten Microdrop Deposition and Solidification. Ph.D. Thesis, Department of Mechanical Engineering, MIT.

Schiaffino, S. & Sonin, A.A. 1997. Molten droplet deposition and solidification at low Weber numbers. *Phys. Fluids* **9** (11), 3172-3187.

Schiaffino, S. & Sonin, A.A. 1997. Motion and arrest of a molten contact line on a cold surface: An experimental study. *Phys. Fluids* **9** (8), 2217-2226.

Schiaffino, S. & Sonin, A.A. 1997. On the theory of the arrest of an advancing molten contact line on a cold solid surface of the same material. *Phys. Fluids* **9** (8), 2227-2233.

Schiaffino, S. & Sonin, A.A. 1997. Formation and stability of liquid and molten beads on a solid surface. *J. Fluid Mech.* **343**, 95-110.

Torresola, J. 1998. Solidification Properties of Certain Waxes and Paraffins. MS thesis, MIT.

Veretennikov, I., Indeikina, A., & Chang H. 1998. Front dynamics and fingering of a driven contact line. *J. Fluid Mech.* **373**, 81-110.

Voinov, O.V. 1978. Asymptote to the free surface of a viscous liquid creeping on a surface and the velocity dependence of the contact angle. *Sov. Phys. Dolk.* **23** (12), 891-893.

Tape 1 CCD Camera																			
Experiment	Plate #	# of drop	time start	time end	Observations	Date	Drop #	time	To	Ti	Ta	S	L (m)	(Theta)a freezing	(Theta)a solidified	hmax (m)	width (m)	Notes
1	1	6	0:00:00	0:03:26	horizontal	9/11/98			70.0	40	22.4	0.31	3.80E-03				3.80E-03	0:03:26 ruler
									70.5	47	22.4	0.21						
									70.4	35	22.4	0.38						
7	2	6	0:03:26	0:25:09	horizontal	9/11/98			70.6	37.2	22.4	0.35						
13	3	8	0:25:09	0:34:58	angle ~ 15	9/13/98			65.0	35	22.5	0.38	6.20E-03		57.4	2.23E-03	4.00E-03	
									65.0	35.2	22.5	0.38						
									70.0	35.2	22.5	0.38						
									70.0	45	22.5	0.24						
									70.0	48.5	22.5	0.19						
									71.5	45.2	22.5	0.24	7.22E-03		36.4	1.33E-03	5.50E-03	
									72.6	47	22.5	0.21						
21	4 & 4bis	8	0:34:58	0:42:42	angle ~ 45	9/13/98	1		70.7	40	22.5	0.31	6.00E-03		52.5	1.60E-03	5.00E-03	
22							2		70.0	50	22.5	0.17						
23						9/14/98	3		72.5	40	23.5	0.31						
24							4		72.5	38.5	23.5	0.33						
25							5		80.6	37	23.5	0.35						
26							6		82.8	36.2	23.5	0.37						
27							7		82.1	35	23.5	0.38	1.30E-02		45.6	1.82E-03	5-3.5-2-3.5 (E-3)	
28							8		87.0	34.3	23.5	0.39						
29	5	10	0:42:42	0:54:09	angle ~ 25	9/14/98			87.6	25	23.5	0.53	6.00E-03		54.4	1.86E-03	4.50E-03	
									86.5	24.3	23.5	0.54						
									86.2	24.5	23.5	0.54						
									90.0	25.1	23.5	0.53						
									92.6	25.3	23.5	0.52	5.00E-03	37.8	52.4	1.90E-03	3.00E-03	solidification end of drop detached from glass
39	6	5	0:54:09	1:01:12	horizontal	9/14/98			90.0	40	23.5	0.31						change in hmax (after sol) = 0.00143 (113.9)
44	7	7	1:01:12	1:11:52	horizontal	9/15/98	1		92.8	39.4	19	0.32	6.23E-03		41.8	2.03E-03	6.23E-03	
45							2		96.0	40	19	0.31						
46							3		97.5	40.1	19	0.31						
47							4		102.0	40.1	19	0.31						
48							5		103.8	40.1	19	0.31	5.99E-03		39.2	1.20E-03	5.99E-03	
49							6		104.1	40	19	0.31	5.35E-03		40.0	1.72E-03	5.35E-03	
50							7		101.9	40.1	19	0.31						
51	8	7	1:11:52	1:26:25	horizontal	9/15/98	1		104.0	40.1	19.5	0.31						
52							2		108.1	40.1	19.5	0.31	5.36E-03		54.0	1.90E-03	5.36E-03	once solidified hmax=0.00144 (115)
53							3		105.3	40.1	19.5	0.31						
54							4		106.0	40	19.5	0.31	5.60E-03		37.6	1.51E-03	5.60E-03	once solidified hmax=0.00107 (85)
55							5		104.8	40	19.5	0.31						
56							6		106.0	40.1	19.5	0.31	6.21E-03		29.8	1.28E-03	6.21E-03	
57							7		106.0	40.1	19.5	0.31						
58	9	10	1:26:25	1:31:58	horizontal		1		105.0	40.1	19.5	0.31						
59							2		108.2	40.1	19.5	0.31						
60							3		106.0	40	19.5	0.31						
61							4		107.0	40	19.5	0.31						
62							5		108.0	40	19.5	0.31						
63							6		107.6	40.1	19.5	0.31						
64							7		107.8	40.1	19.5	0.31						
65							8		107.5	40.1	19.5	0.31	6.19E-03		35.0	1.32E-03	6.19E-03	
66							9		107.8	40.2	19.5	0.31						
67							10		108.0	40	19.5	0.31						
68	10	9	1:31:58	1:43:31	horizontal	9/17/98			100.8	45.5	18	0.23						
									103.5	44	18	0.25						
									115.8	42	18	0.28	6.34E-03		41.0	1.26E-03	6.34E-03	
									109.2	41.3	18	0.29						
									107.0	39	18	0.33						
									112.0	38.2	18	0.34						
									117.8	38.1	18	0.34						
77	11	8	1:43:31	1:53:26		9/21/98			91.0	35.4	17	0.38						
85	12	6	1:53:26	1:59:15	angle ~ 25	9/21/98			103.4	42.1	17	0.28						
91	13	7	1:59:15	2:05:53	angle ~ 25	9/22/98			102.0	53.4	19.5	0.12						
									102.0	53.8	19.5	0.11						
									100.7	45.3	19.5	0.23						
									100.1	41.2	19.5	0.29	1.20E-02	34.5	42.7		6.00E-03	
									102.5	39.6	19.5	0.32						
									103.1	35.2	19.5	0.38	1.10E-02		52.0	1.86E-03	3.50E-03	
98	14	10	2:06:02	2:16:22	angle ~ 25	9/22/98			109.8	39.8	19.5	0.31						
									109.0	40	19.5	0.31						
									106.0	39	19.5	0.33	1.10E-02		43.1	1.42E-03	3.50E-03	
									107.0	40	19.5	0.31						
									105.0	39.8	19.5	0.31	9.00E-03		57.4	1.70E-03	5-3(E-3)	
									106.4	40	19.5	0.31						
									110.2	40.2	19.5	0.31	9.00E-03		39.1	1.76E-03	3-1.5-3.5(E-3)	2:16:22 ruler
108	15	8	2:16:22	2:28:16	angle ~25	9/23/98	1		93.1	41.4	22.5	0.29	6.00E-03	41.6	53.6	1.57E-03	4.50E-03	rough surface (solidified octocosane)

109							2		103.9	38.1	22.5	0.34						
110							3		102.8	35.1	22.5	0.38						
111							4		101.4	35	22.5	0.38						
112							5		102.8	35.1	22.5	0.38						
113							6		102.8	35.2	22.5	0.38						
114							7		101.4	35	22.5	0.38	1.10E-02		56.0	1.72E-03	4.5-3-4.5(E-3)	
115							8		101.0	35.1	22.5	0.38						
116	16	17	2:28:22	2:50:36	angle ~ 25	9/24/98	1		106.5	45.4	23	0.23	7.00E-03		35.7	1.57E-03	5.00E-03	
117							2		105.7	45.3	23	0.23	6.00E-03		48.6	1.54E-03	4.00E-03	
118							3		105.2	43.8	23	0.26						
119							4		107.3	40	23	0.31	9.00E-03		40.5	1.70E-03	4.00E-03	
120							5		107.5	40	23	0.31	6.00E-03		47.5	1.66E-03	4.00E-03	
121							6		107.5	40	23	0.31						
122							7		107.6	40.1	23	0.31						
123							8		107.0	40.2	23	0.31						
124							9		106.7	40	23	0.31						
125							10		106.7	40	23	0.31	8.00E-03		41.0	1.46E-03	4.00E-03	
126							11	2:41:19	106.8	39.9	23	0.31	6.00E-03		63.0	2.18E-03	3.00E-03	
127							12		106.9	39.8	23	0.31						
128							13		107.0	40	23	0.31						
129							14		107.1	40	23	0.31						
130							15		107.3	40	23	0.31						
131							16	2:48:19	107.1	40.1	23	0.31	6.00E-03		64.4	2.07E-03	3.00E-03	
132							17	2:49:35	107.0	40.1	23	0.31	1.10E-02		57.0	1.84E-03	3.5-3-4(E-3)	
133	17	8	2:50:36	2:59:26	horizontal	9/29/98	1		114.0	50	23.8	0.17						influence of height at which the crucible is
134							2	2:54:42	114.5	50	23.5	0.17	6.16E-03		26.6	1.45E-04	6.16E-03	
135							3		115.0	50.1	23.5	0.16						
136					angle ~ 25	10/1/98	4	2:55:52	117.8	45	24	0.24						
137							5		118.0	45	24	0.24						
138							6		118.0	44.9	24	0.24	8.50E-03		47.2	1.27E-03	4.00E-03	
139							7		116.2	45	24	0.24						
140							8		114.3	50	24	0.17	9.00E-03		39.6	1.41E-03	5.00E-03	
141	18	9	3:00:12		angle ~ 25	10/1/98	1		117.0	49.7	24	0.17						
142							2		117.3	54.9	24	0.09						
143							3		119.7	55	24	0.09	9.00E-03		44.4	1.43E-03	5.00E-03	
144							4		117.0	55	24	0.09						
145							5		117.3	55.2	24	0.09						
146							6		116.7	55.1	24	0.09						
147							7		114.5	54.3	24	0.10						
148							8		115.2	55.2	24	0.09						
149							9	3:04:11	117.2	51.9	24	0.14	9.00E-03		48.4	1.47E-03	4.50E-03	

Tape 2 CCD Camera

Experiment	Plate #	# of drop	time start	time end	Observations	Date	Drop #	time	To	Tt	Ta	S	L (m)	(Theta)a freezing	(Theta)a solidified	hmax (m)	width (m)	Notes
150	19	10	0:00:00	0:07:35	angle ~ 45	10/2/98	1		102.0	40.2	22	0.31						0:00:00 scale
151							2		99.8	40.1	22	0.31						
152							3	1:28	95.5	40	22	0.31	9.00E-03	44.0	46.3	1.68E-03	4-3(E-3)	
153							4	2:06	94.5	40	22	0.31	1.60E-02		46.0	2.27E-03	3.5-1.5-3.5(E-3)	
154							5	2:26	97.5	40	22	0.31	9.00E-03		39.1	2.26E-03	3-1.5-3(E-3)	
155							6		97.4	40	22	0.31						
156							7	3:46	97.4	40	22	0.31	1.00E-02		42.2	2.05E-03	3-1.5-2(E-3)	
157							8	4:58	93.6	40	22	0.31	8.00E-03		65.7	2.02E-03	3.5-3(E-3)	
158							9	5:25	92.0	40.1	22	0.31	8.00E-03		59.4	1.71E-03	4-3(E-3)	
159							10	6:19	92.0	40	22	0.31	7.00E-03		71.9	1.98E-03	4.5-3(E-3)	
160	20 bis	11	0:07:35	0:15:33	angle ~ 45	10/5/98	1		91.0	45.5	22	0.23						
161							2		89.7	43.5	22	0.26						
162							3	9:34	92.7	40	22	0.31	1.00E-02	39.5	45.9	2.30E-03	3.00E-03	
163							4	10:34	90.7	40	22	0.31	6.50E-03		58.3	2.18E-03	2.50E-03	
164							5	11:53	90.6	40.1	22	0.31	5.00E-03		67.0	2.10E-03	4.00E-03	
165							6	12:13	89.7	40.1	22	0.31	8.00E-03		52.5	1.96E-03	3.00E-03	
166							7		89.7	39.8	22	0.31						
167							8	13:13	92.3	40.1	22	0.31						
168							9		91.0	40	22	0.31						
169							10	14:45	91.3	39.9	22	0.31	8.00E-03		55.4	2.32E-03	3.00E-03	rough surface (solidified octocosane)
170							11	15:11	91.4	40	22	0.31						
171	21	20	0:15:33	0:34:28	horizontal	10/9/98	1	15:33	92.5	40	22.5	0.31						15:51 - 32:04 droplet deposition on flat plate
172							2		92.3	40	22.5	0.31						32:04 - 34:28 droplet deposition on inclined plate
173							3		92.0	40	22.5	0.31						0:34:21 nozzle dist w/ plate
174							4		91.7	40	22.5	0.31						
175							5		91.4	40	22.5	0.31						
176							6		95.0	40.1	22.5	0.31						
177							7	21:50	95.8	40	22.5	0.31	5.00E-03		44.7	1.58E-03	5.00E-03	
178							8		95.6	40	22.5	0.31						
179							9	23:58	95.8	40	22.5	0.31	4.50E-03		62.4	2.01E-03	4.50E-03	

180							10	:24:49	94.8	39.9	22.5	0.31	5.00E-03		48.1	1.97E-03	5.00E-03	
181							11		96.7	40	22.5	0.31						
182							12		95.4	40.1	22.5	0.31						
183							13		97.6	40	22.5	0.31						
184							14		96.1	40	22.5	0.31						
185							15		98.6	40.1	22.5	0.31						
186							16		97.2	40	22.5	0.31						
187					angle ~ 25		17	:32:27	97.8	40	22.5	0.31	1.20E-02		59.0	2.13E-03	3.5-3-3.5(E-3)	small angle
188					angle ~ 25		18	:32:53	97.9	40	22.5	0.31	5.50E-03		65.4	2.30E-03	3.50E-03	
189					angle ~ 25		19	:33:45	97.2	40	22.5	0.31	7.00E-03		60.1	2.32E-03	3.00E-03	
190					angle ~ 25		20	:34:15	97.5	40	22.5	0.31	8.00E-03		79.8	2.29E-03	3.50E-03	on top of previous one.
191	22	13	0:34:28	0:40:44	angle ~ 45	10/13/98	1	:34:43	95.2	40.1	22.5	0.31						
192							2	:35:16	95.5	40	22.5	0.31	8.00E-03		50.9	1.78E-03	3.00E-03	
193							3	:35:33	97.6	40	22.5	0.31	8.00E-03		49.1	2.01E-03	3.50E-03	
194							4		97.2	40	22.5	0.31						
195							5	:36:06	95.3	40	22.5	0.31	9.00E-03		60.6	1.88E-03	3.50E-03	
196							6	:36:27	95.6	40.1	22.5	0.31	1.80E-02		62.6	1.88E-03	3-2-3-2-3(E-3)	
197							7	:37:05	96.1	40	22.5	0.31	7.00E-03		35.4	1.65E-03	3.00E-03	
198							8	:37:29	96.1	40	22.5	0.31	1.80E-02		46.6	1.54E-03	4-3-2-2.5(E-3)	
199							9	:38:02	96.6	40	22.5	0.31	8.50E-03		58.9	1.75E-03	3.00E-03	
200							10	:38:32	95.4	40	22.5	0.31	8.00E-03		56.6	1.88E-03	3-2-2.5(E-3)	
201							11	:39:02	94.6	40	22.5	0.31	8.50E-03		58.1	1.68E-03	4-2.5(E-3)	
202							12		97.6	39.9	22.5	0.31						
203							13	:40:23	94.4	40	22.5	0.31	8.00E-03		44.4	1.61E-03	3.00E-03	
204	23	16	0:40:44	0:50:11	angle ~ 45	10/15/98	1	:40:54	87.9	40.3	22.6	0.31	6.50E-03		51.5	1.55E-03	3.50E-03	see notes 10/19
205							2	:41:27	86.4	40.1	22.6	0.31	2.15E-02		55.1	2.02E-03	3-2.5-3.5-2-2.5(E-3)	
206							3	:41:47	87.7	40.1	22.6	0.31	7.50E-03		62.3	2.02E-03	2.50E-03	
207							4	:42:30	86.4	40	22.6	0.31	7.00E-03		58.1	1.96E-03	4-2.5(E-3)	
208							5	:43:00	86.8	40	22.6	0.31	6.50E-03		60.1	2.15E-03	3.00E-03	
209							6	:43:27	88.6	40	22.6	0.31						
210							7	:44:00	84.9	40	22.6	0.31						
211							8	:44:33	85.8	40.1	22.6	0.31	6.00E-03		58.7	2.04E-03	2.50E-03	
212							9	:45:02	85.6	40	22.6	0.31						
213							10	:45:29	85.7	40	22.6	0.31	8.00E-03		59.0	2.01E-03	2.50E-03	
214							11	:46:05	86.4	40	22.6	0.31	7.00E-03		58.6	2.09E-03	2.50E-03	
215							12	:46:36	85.6	40	22.6	0.31	7.50E-03		67.3	1.89E-03	2.50E-03	
216							13	:47:16	86.4	40	22.6	0.31	7.50E-03		84.5	1.96E-03	3.00E-03	
217							14	:48:09	87.6	40	22.6	0.31						
218							15	:48:46	86.8	40	22.6	0.31	7.50E-03		55.0	2.03E-03	3.00E-03	
219							16	:49:13	85.9	40.1	22.6	0.31	9.50E-03		63.1	1.89E-03	2.5-1.5-2.5(E-3)	
220	24	13	0:50:11	0:59:03	angle ~ 45	10/22/98	1	:50:52	87.4	35	22	0.38	8.00E-03		47.5	1.85E-03	4-2(E-3)	see notes 10/23
221							2	:51:14	86.2	35	22	0.38						
222							3	:52:23	86.9	35.1	22	0.38						
223							4	:53:44	85.3	35	22	0.38						
224							5	:54:09	87.0	35	22	0.38	8.00E-03		65.5	1.82E-03	4-2(E-3)	
225							6	:54:20	86.5	35	22	0.38	8.00E-03		39.3	1.67E-03	4-2.5(E-3)	
226							7	:55:02	87.3	35	22	0.38						
227							8	:55:58	87.6	35.1	22	0.38						
228							9	:56:19	88.0	35	22	0.38						:56:20 drop # 9 solidified
229							10	:56:31	86.7	34.9	22	0.39	7.50E-03		44.7	1.74E-03	4.5-2.5(E-3)	
230							11	:57:11	87.2	35	22	0.38	1.20E-02		42.8	1.59E-03		
231							12	:58:08	87.5	35	22	0.38	9.50E-03		78.0	1.59E-03	4-1.5(E-3)	
232							13	:58:17	88.0	35	22	0.38	9.50E-03		52.8	1.68E-03	4-2(E-3)	
233	26	20	0:59:03	1:13:25	angle ~ 45	11/12/98	1	:59:03	79.9	34.1	23.1	0.40	9.00E-03		35.7	1.55E-03	6-3(E-3)	solidification end of drop detached from glass
234							2	1:00:41	92.8	33.3	23.1	0.41	1.00E-02		85.3	1.41E-03	6-2(E-3)	solidification end of drop detached from glass
235							3	1:01:00	91.1	33.1	23.1	0.41	8.50E-03		42.5	1.38E-03	5-3(E-3)	
236							4	1:03:55	93.5	32.5	23.1	0.42	8.00E-03		43.1	1.39E-03	4-3(E-3)	
237							5		89.9	32.3	23.1	0.42						touches, wets, and jumps out of screen
238							6	1:04:46	86.8	31.8	23.1	0.43						
239							7		87.4	31.6	23.1	0.43						
240							8	1:06:32	87.9	31.5	23.1	0.43	9.00E-03		39.7			can't make out hmax either
241							9	1:07:02	88.8	31.2	23.1	0.44	7.00E-03		42.5	1.33E-03		
242							10	1:07:27	84.8	30.2	23.1	0.45	9.00E-03		42.6	1.29E-03		
243							11	1:08:07	85.8	30.1	23.1	0.45	8.00E-03		42.8	1.45E-03		
244							12	1:08:45	86.1	30	23.1	0.46	7.50E-03		45.4			can't make out hmax either
245							13	1:09:13	87.1	30.1	23.1	0.45	9.00E-03		43.3	1.57E-03		
246							14	1:09:54	85.0	30	23.1	0.46	1.00E-02		44.9	1.38E-03		
247							15	1:10:08	86.7	30.2	23.1	0.45	8.50E-03		46.5	1.28E-03	4-3(E-3)	
248							16	1:10:19	85.2	55.2	23.1	0.09						
249							17		85.3	55	23.1	0.09						
250							18	1:11:33	84.7	51.1	23.1	0.15	1.30E-02		44.7	1.30E-03	3.50E-03	
251							19	1:12:18	87.7	50.1	23.1	0.16	2.50E-02		39.4	1.29E-03	6-4-3-2.5-3.5(E-3)	
252							20	1:12:50	86.1	50	23.1	0.17			39.4	1.27E-03		
253	31	14	1:13:25	1:31:24	horizontal	1/26/99	1	1:14:09	87.1	55.6	22.5	0.08	6.87E-03		24.3	1.04E-03	6.87E-03	

254							2	1:15:02	88.0	55.7	22.5	0.08	5.91E-03		28.1	1.27E-03	5.91E-03	
255							3	1:16:13	88.3	55.9	22.5	0.08	5.94E-03		30.2	1.22E-03	5.94E-03	
256							4	1:16:52			20.8							thermocouples distances
257							5	1:18:10			20.8							melting of octocosane + capillarity effect
258							6	1:23:58	87.7	65	20.8	-0.05	Can't get total extent on screen		3.2	1.03E-04		measure of equilibrium angle
259							7	1:24:32	89.1	64.9	20.8	-0.05	Can't get total extent on screen		2.5			measure of equilibrium angle
260							8	1:27:13	89.5	65	20.8	-0.05	Can't get total extent on screen		Can't read angle	6.10E-05		calculation of equilibrium angle based on hmax
261							9	1:28:32	89	59.4	20.8	0.03	Can't get total extent on screen		Can't read angle			
262							10	1:29:19	90.2	58.6	20.8	0.04	Can't get total extent on screen		11.3	6.95E-04		important imprecision in the readings
263							11	1:29:36	88.9	58.3	20.8	0.05	Can't get total extent on screen		14.4	8.54E-04		
264							12	1:30:03	87.4	57.3	20.8	0.06	Can't get total extent on screen		23.3	9.51E-04		
265							13	1:30:45	88.9	56.2	20.8	0.08	Can't get total extent on screen		23.3	1.08E-03		
266							14	1:31:14	87.4	56.2	20.8	0.08	6.40E-03		25.6	1.20E-03	6.40E-03	MELTED AWAY RESULTS
267	34	16	1:31:29	1:46:48	angle ~ 45	3/20/99	1	1:33:14	89.5	35	21	0.38	9.00E-03		89.5	1.65E-03	3.00E-03	
268							2	1:34:01	89.5	40.2	21	0.31	1.00E-02		49.3	2.42E-03	3.00E-03	
269							3	1:37:08	89.5	43.9	21	0.25	1.10E-02		50.5	1.50E-03		
270							4		89.5	44.1	21	0.25						
271							5	1:38:56	89.5	44	21	0.25	1.30E-02		61.1	2.07E-03		
272							6	1:40:00	89.5	44.1	21	0.25						
273							7	1:40:27	89.5	44	21	0.25	8.00E-03		43.8	1.44E-03	3.00E-03	
274							8	1:41:50	89.5	47	21	0.21	9.00E-03		46.8	1.61E-03		
275							9	1:42:28	89.5	51.6	21	0.14	1.30E-02		76.9	2.11E-03	5-3(E-3)	
276							10		89.5	50.8	21	0.15						
277							11	1:43:56	89.5	50.9	21	0.15	1.00E-02		53.7	1.37E-03	4.50E-03	
278							12	1:44:08	89.5	51.1	21	0.15	1.00E-02		49.5	1.40E-03	4.5-2.5(E-3)	
279							13	1:44:51	89.5	50.8	21	0.15						
280							14	1:45:00	89.5	50.9	21	0.15						
281							15	1:46:09	89.5	51	21	0.15	1.80E-02		65.5	1.32E-03		
282							16	1:46:39	89.5	50.8	21	0.15	2.30E-02		56.0	1.38E-03		
283	35	20	1:48:14	2:28:41	horizontal	3/24/99	1	1:48:28	87.7	51.2	20.8	0.15	NOT IMPORTANT		47.8	NOT IMPORTANT		continuus flow + crucible very close
284							2	1:50:15	87.9	52.6	20.8	0.13			56.2			only readable thing is theta.
285							3	1:51:32	88.0	53.9	20.8	0.11			48.1			
286							4		87.5	54.1	20.8	0.11						
287							5	1:54:50	87.8	56	20.8	0.08			36.9			
288							6		88.1	56.1	20.8	0.08						
289							7	1:58:51	88.3	57.3	20.8	0.06			27.4			
290							8	2:00:53	87.4	57.5	20.8	0.06			28.7			
291							9	2:03:59	87.7	58.5	20.8	0.04			19.1			
292							10	2:07:06	87.9	59.5	20.8	0.03			18.9			
293							11	2:09:57	87.7	59.3	20.8	0.03			18.7			
294							12	2:13:07	87.5	55	20.8	0.09			31.9			
295							13		87.6	37	20.8	0.35						
296							14	2:18:58	88.0	39.9	20.8	0.31			81.5			
297							15		88.2	41.4	20.8	0.29						
298							16	2:21:44	87.5	44	20.8	0.25			62.6			
299							17		87.8	47	20.8	0.21						
300							18	2:25:01	87.9	47.2	20.8	0.21			59.1			
301							19	2:26:33	87.7	48.7	20.8	0.18			49.4			
302							20	2:28:19	87.9	49.7	20.8	0.17			51.4			
								2:28:44					Plate 27 TOP					
								2:30:17					Plate 19 TOP					
								2:31:09					Plate 22 TOP					
								2:32:09					Plate 30 TOP					
								2:32:44					Plate 36 TOP					

Tape 3 - HSC																		
Experiment	**Plate #**	**# of drop**	**time start**	**time end**	**Observations**	**Date**	**Drop #**	**time**	**To**	**Tt**	**Ta**	**S**	**L (m)**	**(Theta)a freezing**	**(Theta)a solidified**	**hmax (m)**	**width (m)**	**Notes**
303	25	12	0:00:00	10:45	angle ~ 45	11/6/98	1		85.4	40.5	20	0.30						not as good of a lens
304							2		87.1	40	20	0.31						
305							3	1:40	84.6	39.9	20	0.31	6.50E-03		50.9	1.86E-03	3.00E-03	
306							4	1:53	85.0	39.9	20	0.31	8.00E-03		59.1	1.99E-03	5-2.5(E-3)	
307							5	2:29	88.2	40	20	0.31						
308							6	3:04	88.0	40.1	20	0.31						
309							7	3:47	86.5	40.5	20	0.30						
310							8	4:53	86.0	40	20	0.31						
311							9	6:05	87.0	39.8	20	0.31	9.50E-03		48.7	1.38E-03	4-2(E-3)	
312							10	7:27	85.9	39.8	20	0.31	1.70E-02		54.3	2.71E-03	3-2.5 (E-3)	
313							11	8:44	87.2	39.9	20	0.31	2.60E-02		53.0	2.37E-03	2.5-3-2-3-2-3(E-3)	
314							12	10:07	88.0	40	20	0.31						
315	27	9	10:59	23:00	angle ~ 45	11/16/98	1	12:06	87.0	32	22.6	0.43						rec speed 500
316							2	14:44	86.7	32	22.6	0.43	1.00E-02		73.0	1.83E-03	2.50E-03	
317							3	15:54	86.5	32	22.6	0.43	7.00E-03		53.8	1.95E-03	5.00E-03	
318							4	16:16	86.6	32	22.6	0.43	1.05E-02		63.0	1.76E-03	3-2-2.5(E-3)	
319							5	17:53	86.3	32	22.6	0.43	1.70E-02		50.9	2.42E-03	2.5-2-2.5-2(E-3)	

320							6	18:46	85.9	32	22.6	0.43	1.90E-02		51.8	2.48E-03	.5-2.5-2-.5-2-1.5-2(E-3)		
321							7	19:36	87.0	32	22.6	0.43	9.00E-03		48.8	1.78E-03	3-.5-2(E-3)		
322							8	21:55	86.4	32	22.6	0.43	9.50E-03		48.8	1.82E-03	4-1.5-2.5(E-3)		
323							9	22:29	86.6	32	22.6	0.43							
324	28	13	23:08		angle ~ 45	11/16/98	1	23:58	84.4	32.3	22.6	0.42	9.00E-03		47.6	1.40E-03	3-2-3(E-3)		
325							2	25:03	84.4	33.2	22.6	0.41	6.50E-03		57.9	1.50E-03	3.5-2(E-3)		
326							3	25:50	88.0	35.2	22.6	0.38	8.00E-03		47.8	1.99E-03	3.5-2(E-3)		
327							4	27:02	86.3	35.6	22.6	0.38	7.00E-03		53.6	1.75E-03	3.00E-03		
328							5	28:19	86.0	39.7	22.6	0.32							
329							6	29:42	86.9	39.9	22.6	0.31	8.00E-03		49.1	1.74E-03	2.50E-03		
330							7	30:55	85.8	42.2	22.6	0.28	8.50E-03		44.0	1.39E-03	4.5(E-3)		
331							8	31:41	85.0	42.7	22.6	0.27							
332							9	32:42	88.4	44.6	22.6	0.24	9.00E-03		40.5				
333							10	34:57	85.2	47.9	22.6	0.20	1.00E-02		31.6	1.44E-03	4.5-3(E-3)		
334							11	35:45	86.4	48.6	22.6	0.19	1.30E-02		43.4	1.37E-03	5-3-2-3(E-3)		
335							12	36:44	87.5	50.2	22.6	0.16							
336							13	38:05	85.8	50.2	22.6	0.16	8.50E-03		52.5	1.41E-03	4.00E-03		
337	29	9		.44:47	angle ~ 45	11/16/98	1	39:12	85.2	50.7	22.6	0.16							rec speed 500 ID 14
338							2	39:42	85.7	50.2	22.6	0.16	2.30E-02		39.6	1.40E-03	4-3-4-3(E-3)		rec speed 1000 ID 15
339							3	40:13	86	52.4	22.6	0.13							rec speed 1000 ID 16
340							4	40:25	87.4	52.6	22.6	0.13							rec speed 1000 ID 18
341							5	40:52	87.7	52.4	22.6	0.13	1.00E-02		46.7	1.33E-03	5-3(E-3)		rec speed 1000 ID 18
342							6	41:43	86.8	52.6	22.6	0.13	1.00E-02		39.1	1.40E-03	5-4(E-3)		rec speed 1000 ID 19
343							7	42:59	85.3	54.2	22.6	0.10							rec speed 1000 ID 20
344							8	43:35	85.3	54.5	22.6	0.10							rec speed 1000 ID 21
345							9	44:47	85.6	55	22.6	0.09	1.80E-02		41.0	1.39E-03	5-4-3(E-3)		rec speed 1000 ID 22
346	30	12	45:05	59:53	angle ~ 45	11/16/99	1	45:14	86.7	54.8	22.6	0.10							rec speed 1000 ID 1
347					44:50 grayscreen/black screen		2	46:08	87.1	54.6	22.6	0.10							rec speed 1000 ID 2
348							3	46:54	83.4	54.4	22.6	0.10	1.40E-02		47.7	1.43E-03	5-3-4(E-3)		rec speed 1000 ID 3
349							4	47:53	86	54.7	22.6	0.10	1.60E-02		40.1	1.40E-03	5-3(E-3)		rec speed 1000 ID 4
350							5	48:24	86.2	54.5	22.6	0.10	1.60E-02		43.2	1.51E-03	5-3(E-3)		rec speed 1000 ID 5
351					51:48 speed 10		6	50:06	84.5	54.7	22.6	0.10	1.40E-02		39.7	1.41E-03	5-3-3.5(E-3)		rec speed 1000 ID 6
352							7	52:42	87.3	55.6	22.6	0.08	2.15E-02		42.2	1.22E-03	5-3-4(E-3)		rec speed 1000 ID 7
353							8	53:52	88.7	55.5	22.6	0.09							rec speed 1000 ID 8
354							9	55:50	88.1	55.6	22.6	0.08							rec speed 1000 ID 9
355							10	56:29	87.1	55.6	22.6	0.08	1.65E-02	26	40.2	1.33E-03	5-3(E-3)		rec speed 1000 ID 10
356							11	57:56	85.6	55.6	22.6	0.08							rec speed 1000 ID 11
357					58:52 speed 15-10		12	58:29	86.8	55.3	22.6	0.09							rec speed 1000 ID 12
358	32	10	1:00:00	1:01:55	angle ~ 25	2/23/99	1	1:00:18	87.3	55.6	21.3	0.08	CAN'T GET TOTAL EXTENT ON SCREEN BC OF THE CRUCIBLE						rec speed 1000 ID 6 -- top view zigzag
359	33	8	1:01:55	1:05:43	angle ~ 45	2/25/99	1	1:01:59	87.3	42.1	21	0.28	1.30E-02						rec speed 1000 ID 3 -- top view (closer) (extent ~ ap
360							2	1:03:12	89	38.1	21	0.34	1.25E-02				3-2-3(E-3)		rec speed 1000 ID 4 -- top view (extent ~ approxima
361							3	1:03:33	89	46	21	0.22	1.70E-02				3-2-3(E-3)		rec speed 1000 ID 5 -- top view (extent ~ approxima
362							4	1:04:02	89.4	45.5	21	0.23	1.50E-02				4-2.5-3(E-3)		rec speed 1000 ID 6 -- top view (extent ~ approxima
363							5	1:04:59	89	45	21	0.24	1.70E-02						rec speed 1000 ID 7 -- top view (extent ~ approxima
364							6	1:05:18	89	52.8	21	0.13	2.40E-02				4-3-4(E-3)		rec speed 1000 ID 9 -- top view
365							7	1:05:22	87	49.5	21	0.17	1.70E-02				5-2-3-2.5-3(E-3		rec speed 1000 ID 12 -- top view (extent ~ approxin
366							8	1:05:33	87.0	49.5	21	0.17	2.80E-02				6-4.5-5-4-3(E-3		rec speed 1000 ID 14 -- top view (extent ~ approxin
367	36	7	1:05:43	1:10:51	angle ~ 15	10/13/99	1	1:05:50	90	48.2	20.8	0.19	7.50E-03		59.5	1.60E-03			rec speed 1000 ID 2
368					angle ~ 15		2	1:07:23	90	45.1	20.8	0.24	7.00E-03		62.6	1.80E-03	3.5-1.5-2(E-3)		rec speed 1000 ID 3
369					angle ~ 60		3	1:08:02	90	43.1	20.8	0.27	3.50E-02		60.2	2.00E-03	3-2.5-3-2-3(E-3		rec speed 1000 ID 4
370					angle ~ 15		4	1:08:59	90.0	32.1	20.8	0.43	7.50E-03		57.8	3.20E-03			rec speed 1000 ID 6
371					angle ~ 25		5	1:09:13	90.0	32.2	20.8	0.42	1.60E-02		53.3	1.70E-03	4.5-2-2.5(E-3)		rec speed 1000 ID 7
372					angle ~ 15		6	1:09:47	90.0	40	20.8	0.31	7.00E-03		65.0	3.30E-03			rec speed 1000 ID 8
373					angle ~ 15		7	1:10:33	90.0	44.9	20.8	0.24	9.00E-03		47.4	3.10E-03			rec speed 1000 ID 9